

# *BoBBLE: ocean-atmosphere interaction and its impact on the South Asian monsoon*

Article

Published Version

Vinayachandran, P. N., Matthews, A. J., Kumar, K. V., Sanchez-Franks, A., Thushara, V., George, J., Vijith, V., Webber, B. G. M., Queste, B. Y., Roy, R., Sarkar, A., Baranowski, D. B., Bhat, G. S., Klingaman, N. P., Peatman, S. C., Parida, C., Heywood, K. J., Hall, R., Kent, B., King, E. C., Nayak, A. A., Neema, C. P., Amol, P., Lotliker, A., Kankonkar, A., Gracias, D. G., Vernekar, S., Souza, A. C. D., Valluvan, G., Pargaonkar, S. M., Dinesh, K., Giddings, J. and Joshi, M. (2018) BoBBLE: ocean-atmosphere interaction and its impact on the South Asian monsoon. *Bulletin of the American Meteorological Society*, 99 (8). pp. 1569-1587. ISSN 1520-0477 doi: <https://doi.org/10.1175/BAMS-D-16-0230.1> Available at <https://centaur.reading.ac.uk/75355/>

It is advisable to refer to the publisher's version if you intend to cite from the work. See [Guidance on citing](#).

To link to this article DOI: <http://dx.doi.org/10.1175/BAMS-D-16-0230.1>

Publisher: American Meteorological Society

All outputs in CentAUR are protected by Intellectual Property Rights law, including copyright law. Copyright and IPR is retained by the creators or other copyright holders. Terms and conditions for use of this material are defined in the [End User Agreement](#).

[www.reading.ac.uk/centaur](http://www.reading.ac.uk/centaur)

## **CentAUR**

Central Archive at the University of Reading

Reading's research outputs online

# BoBBLE

## Ocean–Atmosphere Interaction and Its Impact on the South Asian Monsoon

P. N. VINAYACHANDRAN, ADRIAN J. MATTHEWS, K. VIJAY KUMAR, ALEJANDRA SANCHEZ-FRANKS, V. THUSHARA, JENSON GEORGE, V. VIJITH, BENJAMIN G. M. WEBBER, BASTIEN Y. QUESTE, RAJDEEP ROY, AMIT SARKAR, DARIUSZ B. BARANOWSKI, G. S. BHAT, NICHOLAS P. KLINGAMAN, SIMON C. PEATMAN, C. PARIDA, KAREN J. HEYWOOD, ROBERT HALL, BRIAN KING, ELIZABETH C. KENT, ANOOP A. NAYAK, C. P. NEEMA, P. AMOL, A. LOTLIKER, A. KANKONKAR, D. G. GRACIAS, S. VERNEKAR, A. C. D'SOUZA, G. VALLUVAN, SHRIKANT M. PARGAONKAR, K. DINESH, JACK GIDDINGS, AND MANOJ JOSHI

A field experiment in the southern Bay of Bengal was developed to generate new high-quality in situ observational datasets of the ocean, air–sea interface, and atmosphere during the summer monsoon.

**T**he Bay of Bengal (BoB) holds a prominent place in the science of monsoons owing to its impacts on the South Asian summer monsoon rainfall and its variability over the countries located along

the rim of the BoB, which is home to over a billion people. Maximum rainfall during the summer monsoon is received in the northeastern BoB and the adjoining land area (Xie et al. 2006). Weather

**AFFILIATIONS:** VINAYACHANDRAN, THUSHARA, GEORGE, VIJITH,\* BHAT, NAYAK, NEEMA, AND PARGAONKAR—Centre for Atmospheric and Oceanic Sciences, Indian Institute of Science, Bangalore, India; MATTHEWS—Centre for Ocean and Atmospheric Sciences, School of Environmental Sciences, and School of Mathematics, University of East Anglia, Norwich, United Kingdom; KUMAR, KANKONKAR, GRACIAS, VERNEKAR, AND D'SOUZA—National Institute of Oceanography, CSIR, Goa, India; SANCHEZ-FRANKS, KING, AND KENT—National Oceanography Centre, Southampton, United Kingdom; WEBBER, QUESTE, HEYWOOD, HALL, GIDDINGS, AND JOSHI—Centre For Ocean and Atmospheric Sciences, School of Environmental Sciences, University of East Anglia, Norwich, United Kingdom; ROY—National Remote Sensing Centre, Indian Space Research Organisation, Hyderabad, India; SARKAR—National Centre for Antarctic and Ocean Research, Esso, Goa, India; BARANOWSKI—Institute Of Geophysics, Faculty of Physics, University of Warsaw, Warsaw, Poland; KLINGAMAN AND PEATMAN—National Centre for Atmospheric Science–Climate, University of

Reading, Reading, United Kingdom; PARIDA—Berhampur University, Odisha, India; AMOL—National Institute of Oceanography, CSIR, Visakhapatnam, India; LOTLIKER AND DINESH—Indian National Centre For Ocean Information Services, Esso, Hyderabad, India; VALLUVAN—National Institute of Ocean Technology, Esso, Chennai, India  
\* **CURRENT AFFILIATION:** School of Marine Sciences, Cochin University of Science and Technology, Kochi, India  
**CORRESPONDING AUTHOR:** P. N. Vinayachandran, vinay@iisc.ac.in

*The abstract for this article can be found in this issue, following the table of contents.*

DOI:10.1175/BAMS-D-16-0230.1

In final form 23 January 2018

©2018 American Meteorological Society

For information regarding reuse of this content and general copyright information, consult the [AMS Copyright Policy](#).

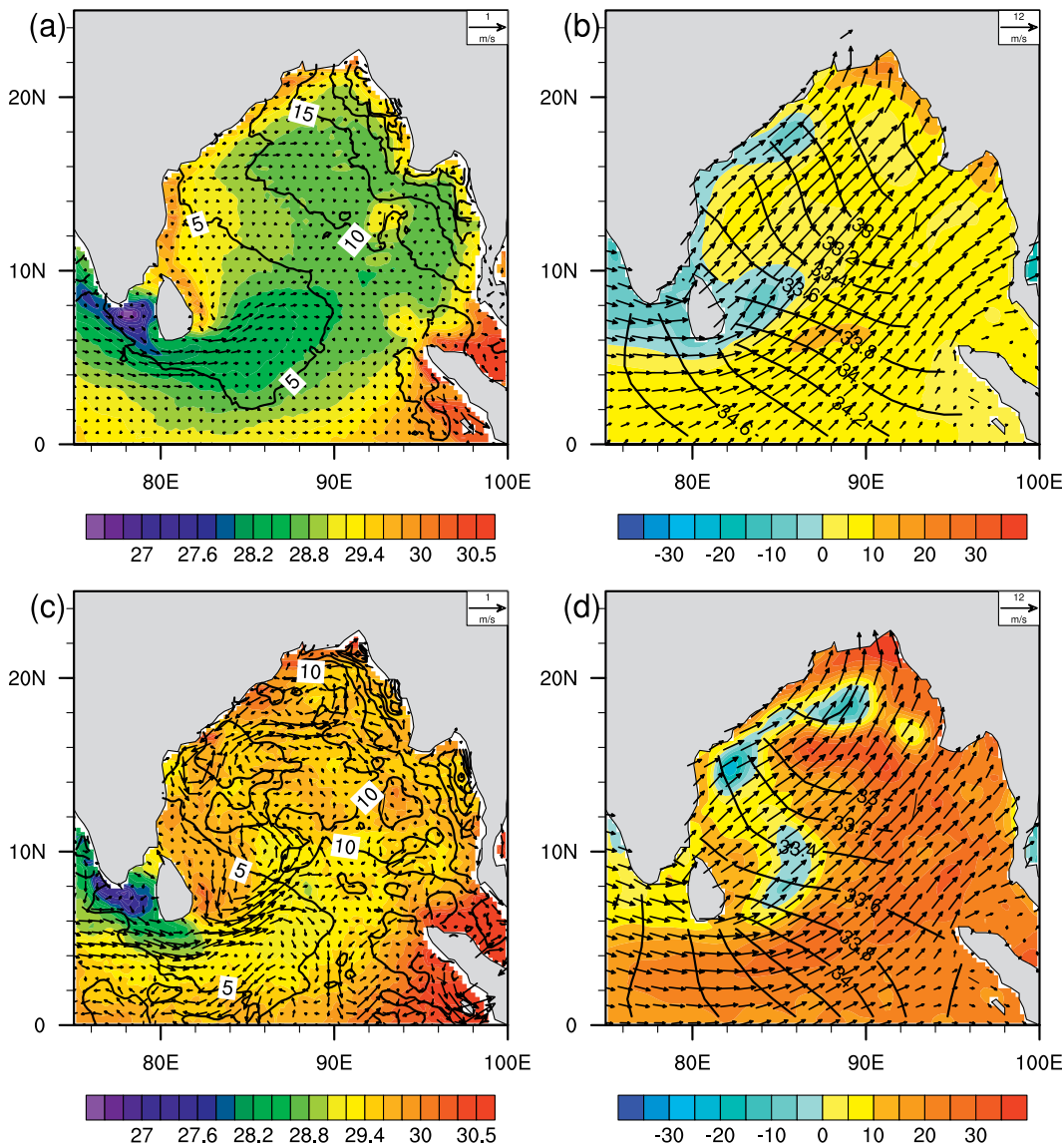


**FIG. 1. Climatology for the period 23 Jun–24 Jul. (a) Tropical Rainfall Measuring Mission (TRMM) Microwave Imager (TMI) SST (1998–2014, shading, °C), TRMM rainfall (1998–2015, contours), and Ocean Surface Current Analysis–Real Time (OSCAR; 1993–2015, vector arrows). (b) Archiving, Validation, and Interpretation of Satellite Oceanographic Data (AVISO) MSLA (1993–2015, shading, cm), salinity from Argo (2005–15, contours), and Advanced Scatterometer (ASCAT) surface winds (2008–15, vector arrows). (c),(d) As in (a) and (b), respectively, but for the period 23 Jun–24 Jul 2016.**

systems that form over the BoB contribute substantially to rainfall over central India (Gadgil 2003). Several such systems breed over the BoB during each monsoon season because of the capacity of the BoB to recharge its sea surface temperature (SST) quickly in the short sunny spells after the passage of each disturbance (Shenoi et al. 2002; Bhat et al. 2001). This rapid SST warming is facilitated by the thin mixed layer maintained by freshwater input from rainfall and river runoff into the BoB (Vinayachandran et al. 2002). These general features characterize the BoB north of about 15°N.

Farther south, features of the ocean–atmosphere system are somewhat different (Matthews et al. 2015), yet intriguing. Climatologically, both the ocean and atmosphere show contrasts between east and west. The SST is marked by a cold pool (Joseph et al. 2005; Das et al. 2016) around Sri Lanka (Fig. 1a) compared to the warmer water in the east. The sea surface salinity (SSS; Fig. 1b) is higher in the west than in the east (Vinayachandran et al. 2013). Most remarkably, the western part of the southern BoB is marked by the intense monsoon current that flows into the BoB carrying higher-salinity Arabian Sea Water. The



atmosphere above the cold pool is characterized by a minimum in seasonal total rainfall (Fig. 1a) and has the lowest amount of low-level clouds in the region (Shankar et al. 2007; Nair et al. 2011). The role of ocean dynamics and air–sea interaction processes in defining these large zonal and meridional variations and the impact of these on monsoon rainfall elsewhere have received little attention.

Several field experiments have been conducted in the BoB to understand the response of the BoB to monsoons and its possible feedbacks (Bhat and Narasimha 2007). Among the recent experiments, the Bay of Bengal Monsoon Experiment (BOBMEX; Bhat et al. 2001) focused on the coupled ocean–atmosphere system in the northern BoB during the peak monsoon months of July–September. The Joint Air–Sea Monsoon Interaction Experiment (JASMINE) sampled the eastern Indian Ocean and southern BoB during May and September 1997 (Webster et al. 2002). The Continental Tropical Convergence Zone (CTCZ) experiment carried out under the Indian Climate Research Program made observations of both the southern and northern BoB during 2009 and 2012 (Rao et al. 2011; Vinayachandran et al. 2013; Jain et al. 2017). The Air–Sea Interaction Research Initiative (ASIRI) campaign covered both summer and winter monsoons and combined datasets from multiple platforms and model simulations (Wijesekera et al. 2016b). These experiments have contributed significantly toward our understanding of the processes at work during monsoons, but a large gap exists in our knowledge base about the physical processes in the southern BoB. The BoB Boundary Layer Experiment (BoBBLE) focuses on the less known, yet important, southern BoB and combines observations from multiple instruments, including five ocean gliders, to obtain high-quality time series observations of the ocean, air–sea interface, and atmosphere during the peak period of the 2016 summer monsoon.

The first set of measurements in the region was carried out by Schott et al. (1994) using current meter moorings and ship sections in the early 1990s, which provided a description of the annual cycle and

intraseasonal variation of monsoon currents. Earlier hydrographic surveys (Murty et al. 1992) indicated the flow of high-salinity water into the southern BoB. The intrusion of the summer monsoon current (SMC) into the BoB was described using geostrophic currents derived from expendable bathythermograph (XBT) datasets (Vinayachandran et al. 1999). The seasonal cycle and interannual variability of the thermocline along 6°N was explored using the XBT data (Yu 2003). Using shipboard observations made during the CTCZ field campaign, Vinayachandran et al. (2013) described the existence of a salt pump in the southern BoB. Using acoustic Doppler current profiler (ADCP) moorings, Wijesekera et al. (2016c) obtained current measurements from east of Sri Lanka for nearly two years. Lee et al. (2016) reported observations using multiple platforms, as a way to understand the circulation and transport around Sri Lanka. Sustained ocean observation systems, the Research Moored Array for African–Asian–Australian Monsoon Analysis and Prediction (RAMA; McPhaden et al. 2009) in particular, have also contributed to the database in this region. However, there is a major gap in the observations that are relevant to understanding the complete ocean–atmosphere system during the summer monsoon.

The primary objective of the BoBBLE field program was to characterize the ocean–atmosphere system in the southern BoB, which is marked by contrasting features in its eastern and western regions. One of the major aims is to generate new high-quality in situ observational datasets of the ocean, air–sea interface, and atmosphere during the peak phase of the summer



**FIG. 2.** *R/V Sindhu Sadhana* of CSIR National Institute of Oceanography, Goa, India, which was used for the BoBBLE field program.

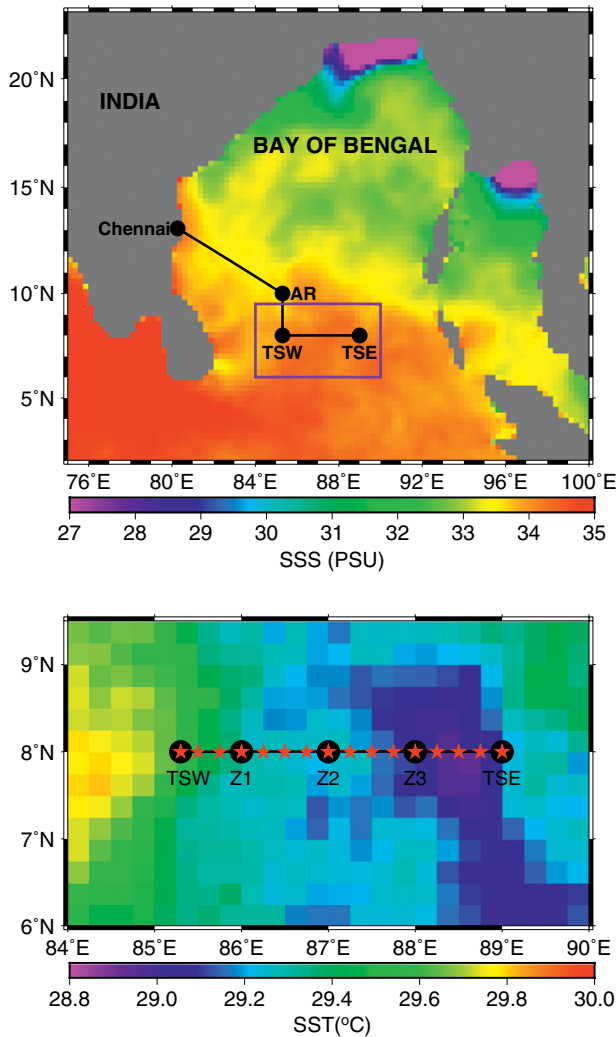


**FIG. 3. (top)** A map of the BoB and the cruise track of the BoBBLE field program. SSS (shading) is from SMAP. **(bottom)** The section along which observations were made during BoBBLE. The positions (black circles of TSW, Z1, Z2, Z3, and TSE) represent glider deployment locations (see Table 1 for details). Argo float deployments (see Table 2 for details), IOP, radiometer, and VMP profiling as well as water sampling were also carried out at these locations. Stars indicate locations where additional CTD profiles were measured during the return leg of the cruise. At TSE, additionally, CTD profiles were measured from 4 to 15 Jul 2016. Shading indicates SST from Advanced Microwave Scanning Radiometer for Earth Observing System (AMSR-E).

collected during the BoBBLE field program, the details of which are given in the next section. The “Meteorology and air–sea interaction” section and the “Oceanographic features of the southern BoB” section describe air–sea interaction and the oceanographic features of the southern BoB, respectively. We conclude with a summary and outlook.

**BoBBLE FIELD PROGRAM.** The Research Vessel (R/V) *Sindhu Sadhana* (Fig. 2) sailed from the port of Chennai, Tamil Nadu, India, on 24 June and returned on 23 July 2016. The BoBBLE cruise was conducted along the track shown in Fig. 3. Shipboard observations can be classified into two types: observations made along the 8°N section from 85.3° to 89°E in the international waters of the southern BoB and time series observations were at 8°N, 89°E (referred to as TSE) for a period of 10 days, 4–15 July 2016. Ocean glider deployments provided similar time series at locations marked as black circles in Fig. 3.

Two shipboard ADCPs (operating at frequencies of 38 and 150 kHz), an automatic weather station (AWS), and a thermosalinograph recorded data continuously during the cruise period. A Sea-Bird Electronics (SBE) 911plus conductivity–temperature–depth (CTD) profiler measured vertical profiles and collected water samples at all points marked as stars in Fig. 3. Nominally, the casts were to a depth of 1,000 m. At selected stations additional CTD casts extended all the way to the deep ocean floor. At TSE, CTD

monsoon. The overarching objectives of BoBBLE are to evaluate the role of ocean–atmosphere interactions in the simulation and prediction of the summer monsoon, to combine data and models to investigate the physical and biogeochemical processes under the monsoon forcing, and to determine the role of the abovementioned processes in causing the synoptic-scale variability of the South Asian monsoon system.

The aim of this paper is to make the community aware of the new dataset that has been acquired and to present a preliminary analysis of the observations

**TABLE 1. Ocean glider deployments during the BoBBLE cruise. ID = identification.**

Glider ID	Waypoint	Deployed	Recovered	Instrumentation
SG579	8°N, 86°E, then 8°N, 85°20'E	30 Jun	20 Jul	CTD, dO <sub>2</sub> , Chl, backscatter, PAR
SG534	8°N, 87°E	1 Jul	17 Jul	CTD, dO <sub>2</sub> , Chl, backscatter
SG532	8°N, 88°E	2 Jul	16 Jul	CTD, dO <sub>2</sub> , Chl, backscatter
SG620	8°N, 88°54'E	3 Jul	14 Jul	CTD, dO <sub>2</sub> , Chl, backscatter
SG613	8°N, 89°06'E	4 Jul	15 Jul	CTD, microstructure shear, and temperature

**TABLE 2. Argo float deployments during the BoBBLE cruise.**

No.	Argo float ID	Date	Time (UTC)	Lat (°N)	Lon (°E)	Notes
1	Navis OCR 0629	28 Jun 2016	1145	8	85.3	Daily profile surfacing at 1200 UTC
2	Apex STS 7599	30 Jun 2016	0910	8.04	86.05	Daily profile surfacing at 1500 UTC
3	Apex STS 7598	30 Jun 2016	0910	8.04	86.05	Daily profile surfacing at 0300 UTC
4	Navis OCR 0631	1 Jul 2016	1410	8.07	87.04	Daily profile surfacing at 1200 UTC
5	Apex STS 7597	1 Jul 2016	1410	8.07	87.04	Daily profile surfacing at 1500 UTC
6	Apex STS 7596	2 Jul 2016	0615	8	88	Daily profile surfacing at 1500 UTC
7	Navis OCR 0630	4 Jul 2016	1323	8.06	89.02	Daily profile surfacing at 1200 UTC

observations were carried out to a depth of 500 m at approximately 3-hourly intervals, with a once-daily profile to 1,000 m. Four standard MetOcean drifting buoys were also deployed during the BoBBLE field program.

Five ocean gliders were deployed during 1–19 July 2016 along the 8°N transect (Table 1). All gliders were equipped with a CTD package, enabling measurements of temperature and salinity with 0.5–1-m vertical resolution from the surface to 1,000-m depth. Four gliders were equipped with dissolved oxygen (dO<sub>2</sub>), chlorophyll fluorescence (Chl), and optical backscatter sensors. Additionally, one glider (SG579) was equipped with a photosynthetically active radiation (PAR) sensor, and another (SG613) with microstructure shear and temperature sensors. Individual dives lasted 3–4 h. In total, 462 dives were made. Optimally interpolated (OI) two-dimensional (depth, time) gridded datasets (Matthews et al. 2014) were produced for each glider. The radii of influence in the Gaussian weighting functions were 2 m and 3 h. The five depth–time OI datasets were then further combined into a single three-dimensional longitude–depth–time dataset, by linear interpolation in longitude, taking into account the movement of the gliders with time.

Seven Argo floats were deployed in the BoB along 8°N, between 85.3° and 89°E (Table 2). As BoBBLE is designed to target surface processes, all floats were programed to provide daily high-resolution profiles of the top 500 m in a region where in situ surface data are scarce. A second OI dataset was created using profiles from core Argo floats from the international Argo program, BoBBLE Argo floats, glider profiles, and the shipboard CTD. These OI data were mapped using World Ocean Database climatology (Boyer et al. 2013) and gridded at 25 longitude grid points at 8°N, from 83° to 95°E at 0.5° intervals. The time grid ran from 1 June 2016, before the BoBBLE field campaign started, to 30 September 2016, with data from each day gridded separately. This combined OI

dataset covers a longer period than the BoBBLE field program, as there was a continuous Argo float presence in the BoB before the BoBBLE campaign, which was then significantly enhanced by the seven floats deployed during BoBBLE.

To map mesoscale and submesoscale features, a Teledyne Oceanscience Underway CTD (uCTD), fitted with SBE conductivity–temperature (CT) sensors, was used for measuring temperature and salinity profiles while the ship was sailing at a speed of 6 kt (3.06 m s<sup>−1</sup>). Nominally, the uCTD probe was allowed to profile vertically for 2 min in order to achieve a drop rate of about 1.5–2.5 m s<sup>−1</sup>, covering a depth range of approximately 250 m, and the data were binned at 1-m depth intervals.

A vertical microstructure profiler (Rockland Scientific VMP-250) comprising two shear probes, one set of high-resolution microtemperature and conductivity sensors and another set of standard CTD sensors, was operated at all glider stations along the transect as well as at TSE. At each station, two to three profiles were measured. At TSE, profiles were measured at 0000, 0400, 0800, 1200, and 1700 UTC each day. In total, 138 casts were made, including that at TSE.

To characterize the surface and subsurface light field, bio-optical measurements were carried out with a Satlantic HyperPro II hyperspectral underwater radiometer (HUR) equipped with three sensors for light, an SBE Environmental Characterization Optics (ECO) triplet for fluorescence and colored dissolved organic matter (CDOM), and CTD sensors. The light sensors measured downwelling, upwelling, and total solar irradiance. The HUR was operated for 17 days under cloud-free conditions between 0600 and 0700 UTC at TSE, and along the 8°N transect between 0530 and 0800 UTC. A total of 37 profiles were collected during BoBBLE. An inherent optical profiler (IOP) was used for the measurement of light absorption and scattering coefficients, backscattering coefficient, chlorophyll-a, CDOM, turbidity, and PAR along with a CTD sensor.

The IOP was operated at TSE at 0130 and 0830 UTC each day.

The meteorological measurements included an AWS, an air–sea flux observing system (Table 3), and radiosondes. A LI-COR infrared gas analyzer in conjunction with the 3D sonic anemometer–based eddy covariance system and high-frequency response ship motion sensors were installed at the bow, at a height of approximately 15 m above the sea surface and 6 m above the fore-castle deck. Sensible and latent turbulent heat fluxes are estimated using the eddy covariance method (Fairall et al. 1997; Edson et al. 1998; Dupuis et al.

TABLE 3. Details of shipboard meteorological instruments. Surface variables, including air temperature, SST, relative humidity, pressure, and all four components of radiation, wind speed and direction, rain rate, and ship position, were continuously monitored by the AWS. Surface variables were sampled at 10-s intervals, and 1-min averages (including true wind speed and direction) were stored. The ship’s SBE SST sensor was placed at a depth of approximately 3.5 m below sea level (Weller et al. 2008).			
Parameter	Range	Mean accuracy	Resolution
Wind speed (R. M. Young)	0.7–50 m s <sup>−1</sup>	0.2 m s <sup>−1</sup> or 2%	0.1 m s <sup>−1</sup>
Wind direction (R. M. Young)	0°–360°	3°	1°
Air temperature (YSI)	0°–45°C	0.2°C	0.05°C
Relative humidity (Rotronic)	0%–100%	2%	0.5%
Atmospheric pressure (Honeywell)	850–1,050 hPa	0.1 hPa	0.01 hPa
Optical rain gauge (Optical Scientific)	0–50 mm h <sup>−1</sup>	0.4 mm h <sup>−1</sup>	0.25 mm
Radiation (shortwave) (LI-COR)	0–300 mW cm <sup>−1</sup>	5%	—
SST (SBE)	0°–35°C	0.1°	0.05°C

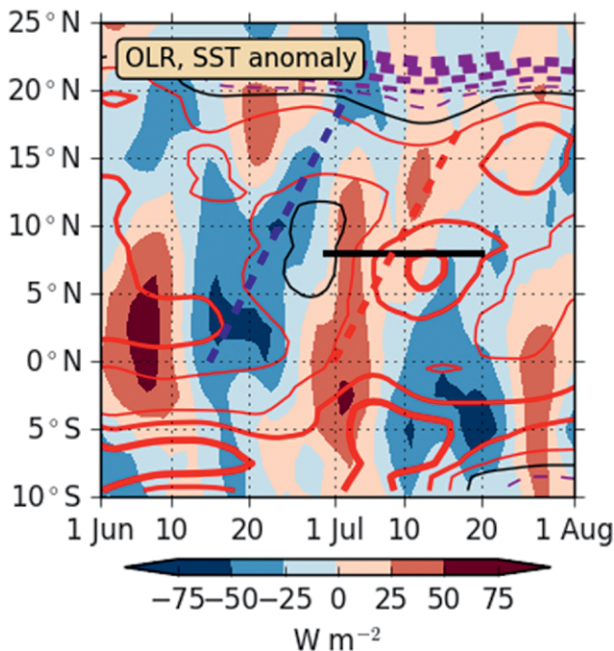


**FIG. 4.** Hovmöller diagram (averaged from 80° to 95°E) for anomalous 5-day running mean outgoing longwave radiation (OLR; shading interval: 25 W m<sup>−2</sup>), SST (line contour interval: 0.2°C; negative contours: dashed purple, zero contour: solid black, positive contours: solid red). The line at 8°N shows the timing of the BoBBLE ship and glider and Argo float deployments (solid black). Negative (positive) OLR anomalies indicate convectively active (suppressed) phase of BSISO. The main axis of northward propagation of the active (dashed blue) and suppressed (dashed red) phases of the BSISO during Jun–Jul 2016.

2003). Upper-air observations of temperature, pressure, humidity, and wind were taken with Vaisala RS92 radiosondes, launched nominally at 0000 and 1200 UTC every day. Additional launches were also made on some days to capture the diurnal cycle.

**METEOROLOGY AND AIR–SEA INTER-ACTION.** Large-scale conditions over the BoB during summer 2016. The all-India rainfall for 2016 had a 3% deficit relative to climatology ([www.imd.gov.in](http://www.imd.gov.in)), ENSO conditions were near neutral, and SST anomalies in the tropical Pacific and Indian Oceans were modest ([www.ospo.noaa.gov](http://www.ospo.noaa.gov)). The Indian Ocean dipole (Saji et al. 1999) was in a negative state, with slightly warmer-than-usual conditions in the eastern Indian Ocean and cooler-than-usual conditions in the west, representing an intensification of the usual cross-basin gradient. Despite this, 2016 can be seen as a representative monsoon season and is therefore ideally suited for investigating its link with conditions in the BoB.

The mean monsoon winds during the observation period were steady southwesterlies (Fig. 1d) and the SMC was intense with an axis oriented in the southwest–northeast direction, to the east of Sri Lanka (Fig. 1c). The mean SST was relatively cooler around the SMC with warmer water farther to the west and east. The east–west SST contrast that is typically seen in the climatology (Fig. 1a) was not as well developed during the period of observations (Fig. 1c). The mean SSS pattern was comparable to climatology (Figs. 1b,d).

Intraseasonal variability had a significant effect on the conditions observed during the BoBBLE



campaign. In June 2016 the southern BoB was under the influence of a convectively active phase (Fig. 4) of the boreal summer intraseasonal oscillation (BSISO) (Lee et al. 2013). This propagated northward (dashed blue line in Fig. 4) and was replaced by a convectively suppressed phase of the BSISO during July 2016. Toward the end of the deployment, conditions returned to the convectively active phase with the incursion of the next cycle of the BSISO. Hence, the main BoBBLE deployment sampled the transition between the end of one active BSISO event, the subsequent suppressed phase, and the initiation of the active phase in the following BSISO event. This is an ideal framework for analyzing the high-resolution in situ observations made during the BoBBLE cruise.

*In situ measurements of air–sea interaction.* The time series of surface fluxes and atmospheric and ocean surface conditions observed from the ship are described here, within the large-scale context of the suppressed phase of the BSISO in the southern BoB. The focus is on the period 4–15 July 2016 when the ship was at TSE (Fig. 5a). During this period no precipitation was observed. Cloud conditions were characterized by broken layers of mid- and high-level clouds and scattered small cumulus, with a generally high surface solar radiation flux. The surface wind speeds during the first half of the period were 8–10 m s<sup>−1</sup> (Fig. 5d), typical for the southern BoB during the summer monsoon. However,

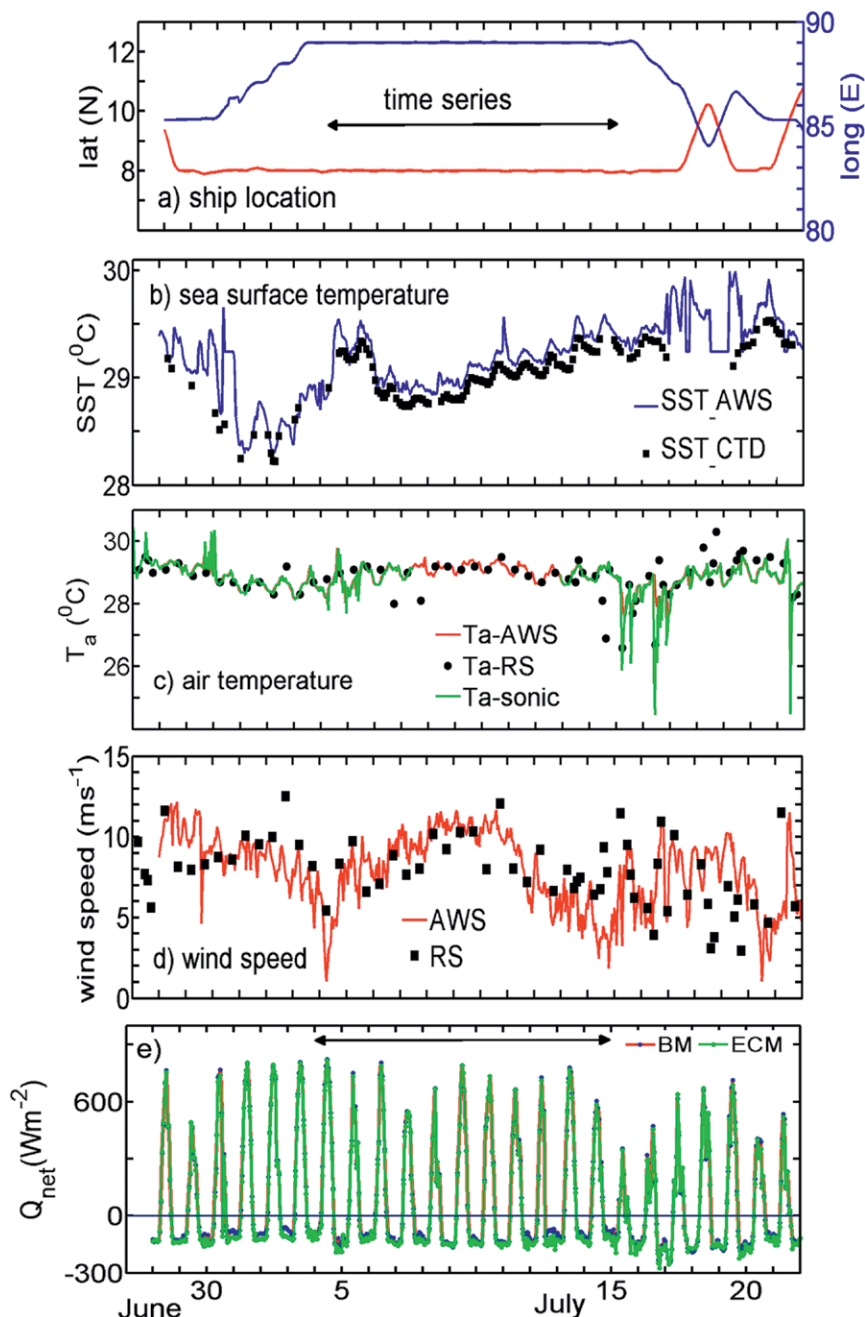


**FIG. 5.** (a) Ship position as a function of time. Latitude (red line) and longitude (blue line) are marked. The double-headed arrow shows the time series observation period at TSE (8°N, 89°E). (b) SST from AWS and CTD at 3.4-m depth. (c) Air temperature. (d) Surface (approximately 10 m) wind speed (red line) and radiosonde wind speed (black squares) at 975 hPa. (e) Surface net heat flux into the ocean. RS is radiosonde, Ta-sonic is sonic anemometer temperature corrected for water vapor, and ECM and BM refer to turbulent fluxes calculated using the eddy covariance and bulk methods, respectively; refer to text for other abbreviations.

in the latter half of the period, they decreased to 5 m s<sup>−1</sup> or below, with an associated reduction in the (cooling) surface latent heat flux.

The high solar radiation flux and relatively low latent heat flux are consistent with conditions that prevail during the suppressed (calm, clear) phase of

the BSISO (Lee et al. 2013). Consequently, the net heat flux into the ocean was positive (Fig. 5e). This led to a steady increase in SST, from 28.0° to 29.5°C (Fig. 5b),

again consistent with the developing oceanic conditions typically found in the suppressed BSISO phase. Surface atmospheric temperature (Fig. 5c) increased in pace with the SST.

Deep atmospheric convection broke out at the end of the TSE period. From 16 July 2016 onward, deep convective cloud systems with intense precipitation, associated with the next active BSISO phase, were observed from the ship. It should be noted that at this time, the ship had departed TSE and was cruising westward on the return leg of the 8°N section (Fig. 5a); hence, the sampling of these precipitating systems was not at a fixed location. This deep convection was part of the next active BSISO phase (Fig. 4).

The change in atmospheric characteristics from suppressed to active convection can clearly be seen in the shipboard AWS time series. The most notable change is that air temperature dropped on 15 July and remained significantly lower than SST from then on (Figs. 5b,c). The air temperature was much more variable, with spikes of low temperature followed by a gradual recovery. Low-temperature spikes are due to evaporation from falling raindrops in the subcloud layer and formation of a pool of cold air near the surface (i.e., wet-bulb effect). Surface wind speed increases from its minimum on 15 July (Fig. 5d) and shows large

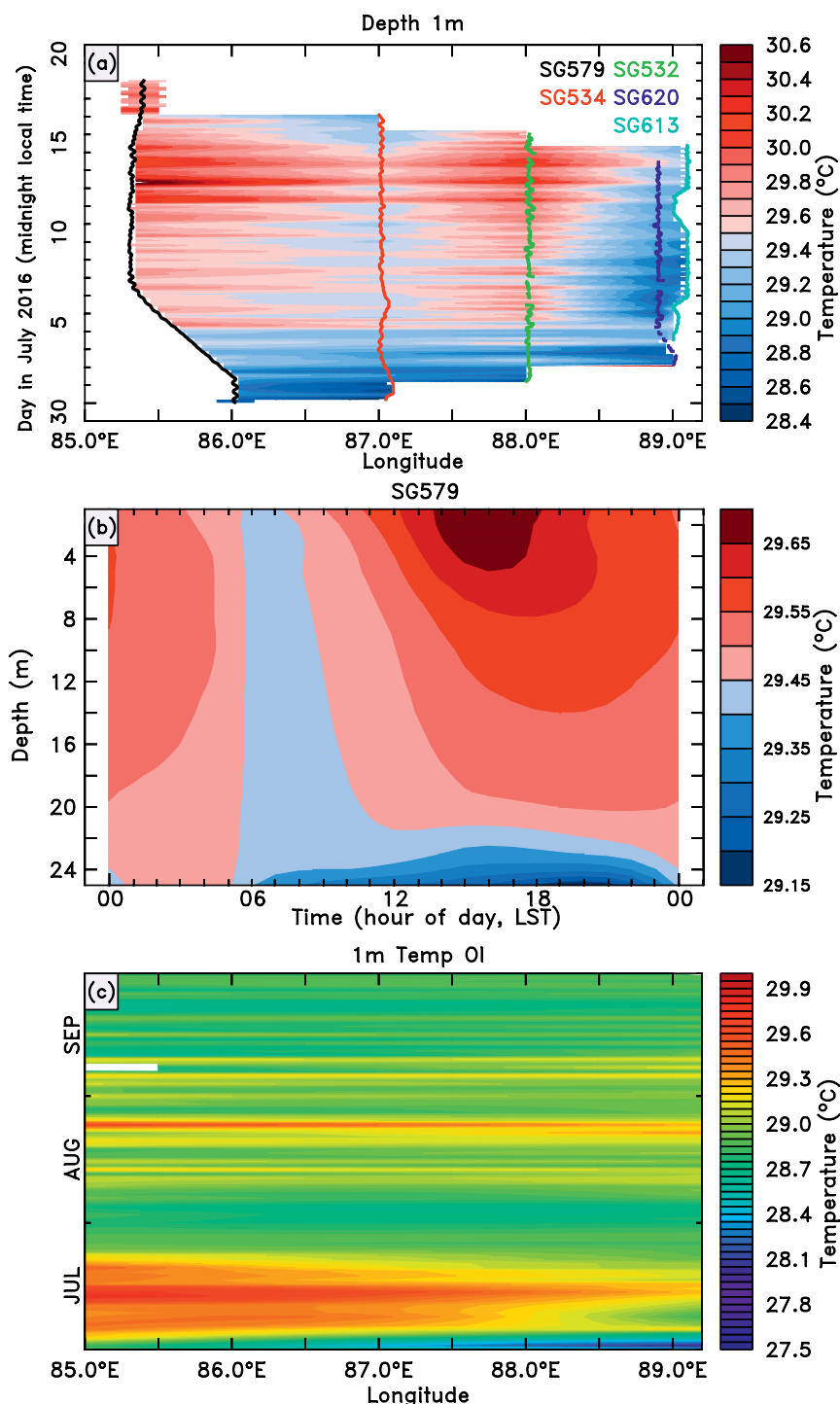


**FIG. 6.** (a) Longitude–time section of OI glider temperature at 1-m depth. The longitudes of the five gliders are shown (colored lines). (b) Average diurnal cycle of temperature for glider SG579 at the western end of the 8°N section. Time of day is in local solar time (LST). (c) Longitude–time section of temperature at 1-m depth for Jul–Sep 2016, based on OI Argo data. A 3-day moving mean has been applied to the Argo data.

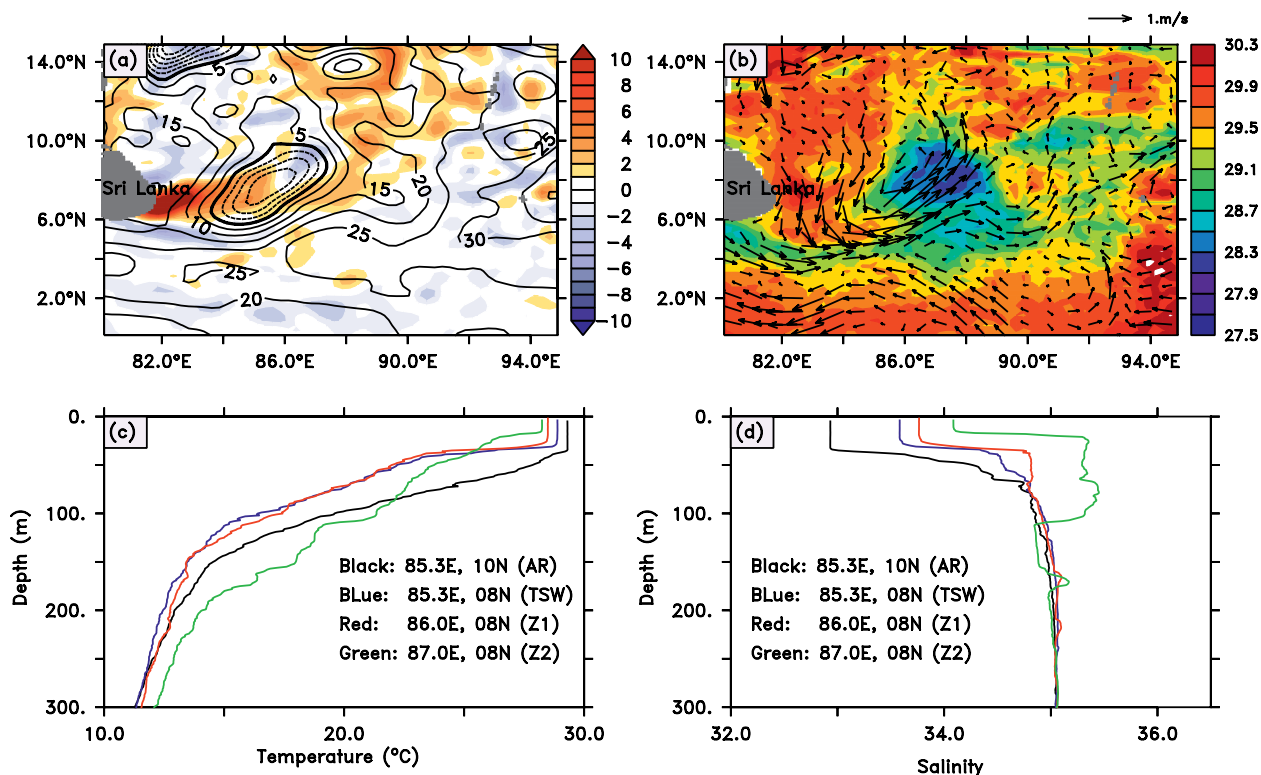


**FIG. 7.** Sri Lanka dome. (a) AVISO MSLA (cm) for 30 Jun 2016 (contours) and wind stress curl (shading,  $\text{N m}^{-3}$ ) from ASCAT averaged for the period 20 Jun–1 Jul 2016. (b) AMSR-E SST (shading,  $^{\circ}\text{C}$ ) averaged for the period 27–30 Jun 2016 overlaid on current vectors ( $\text{m s}^{-1}$ ) from OSCAR for 2 Jul 2016. (c) Temperature and (d) salinity profiles that contrast the spatial structure of the SLD. Profiles were measured at a location to the north (black) and east of the SLD (green), and inside the SLD (blue, red). Refer to Fig. 3 for the locations. Salinity profiles show that the high-salinity core of the SMC (green curve) is absent in the regions of the SLD (blue and red).

variability. These are also likely due to gusts of cold, dry air originating from the convective systems associated with the transition to an active phase of BSISO.

Overall, the shipboard measurements comprehensively captured the transition from the atmospheric convectively suppressed phase of the BSISO during 4–15 July to the following convectively active phase.

Glider measurements extend the analysis of air–sea interaction along the entire  $8^{\circ}\text{N}$  section. The longitude–time section of ocean temperature at 1-m depth (Fig. 6a) clearly shows the gradual warming across the whole section from approximately  $28.5^{\circ}\text{C}$  on 3 July to up to  $30.5^{\circ}\text{C}$  on 13 July. Superimposed on this are strong diurnal fluctuations, especially at the westernmost glider (SG579) and  $88^{\circ}\text{E}$  (SG532). These represent the formation of surface diurnal warm layers (Fig. 6b) that were previously diagnosed in the Indian Ocean by an ocean glider (Matthews et al. 2014).

Argo floats extend the analysis even further to the end of the season. With the onset of the next active phase of BSISO in mid-July, the temperature rapidly

decreased (Fig. 6c) followed by a weaker warming from mid-August to mid-September and a further cooling.

## OCEANOGRAPHIC FEATURES OF THE SOUTHERN BoB.

The deployment of multiple platforms has yielded an unprecedented description of the oceanographic features of the southern BoB during the summer monsoon. In particular, a nearly one-month time series of physical and biogeochemical variables along a zonal section at  $8^{\circ}\text{N}$  has been obtained. This section describes these features briefly.

**SLD.** The cyclonic circulation feature located to the east of Sri Lanka, caused by cyclonic wind stress curl above the Sri Lanka dome (SLD; Fig. 7a), which is associated with the doming of the thermocline (Vinayachandran and Yamagata 1998; Wijesekera et al. 2016a). The SLD during BoBBLE is seen as a patch of negative mean sea level anomalies (MSLA; Fig. 7a), enclosed by the zero MSLA contour (thick line). The SLD was well developed during the survey with cyclonic circulation and cooler SST around it (Fig. 7b). The CTD profiles measured during BoBBLE captured the doming of the

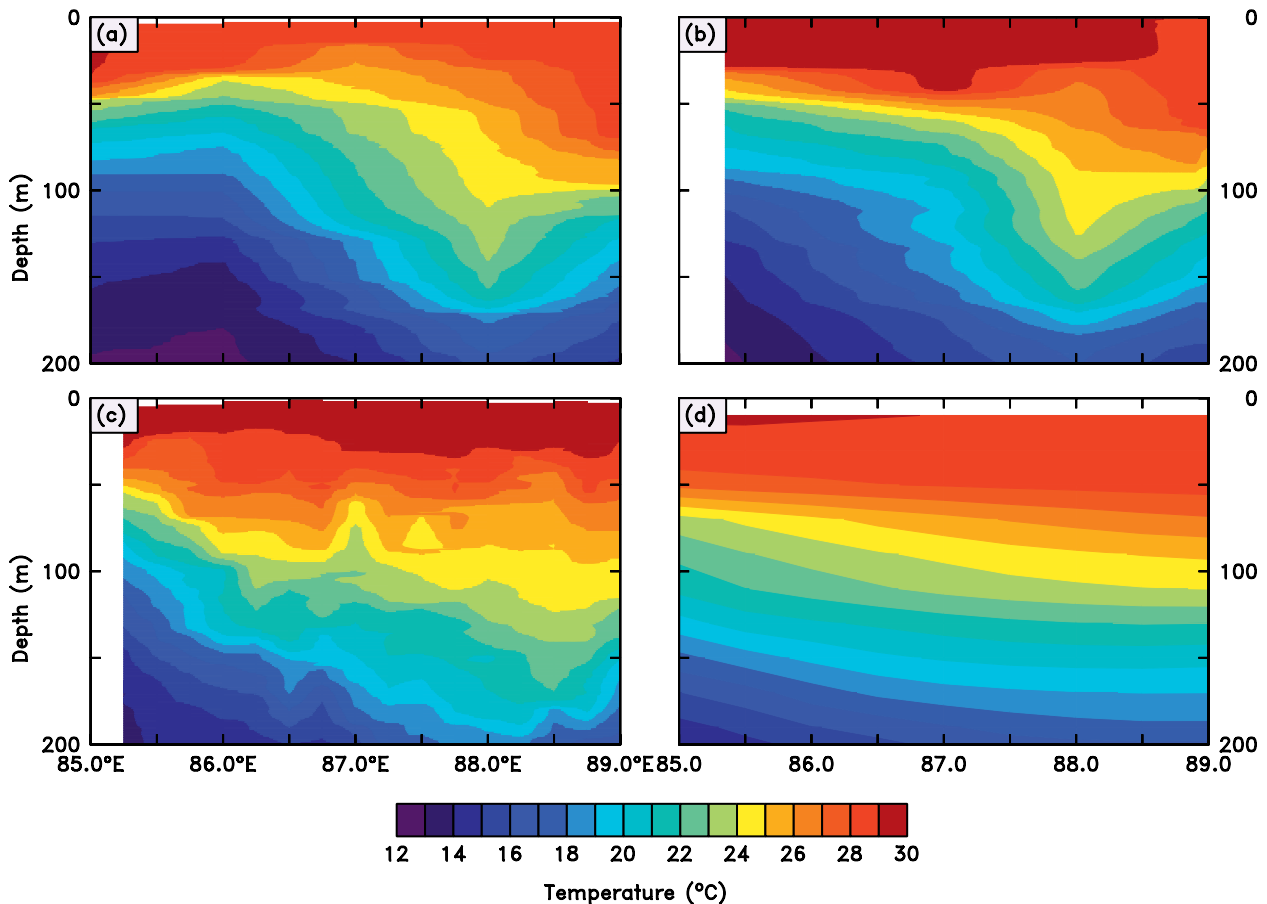


**FIG. 8.** Longitude–depth sections of temperature along 8°N using (a) CTD section during 30 Jun–4 Jul 2016, (b) glider data on 8 Jul 2016, (c) CTD section observed during 15–20 Jul 2016, and (d) OI Argo data on 24 Jul 2016.

thermocline with respect to its exterior. On 28 and 30 June 2016, CTD profiles were measured at locations within the SLD, and on 1 July 2016 on its outer edge. A comparison of these profiles shows that the thermocline (taken as the depth of the 20°C isotherm; D20) within the dome is about 30 m shallower compared to its exterior (Fig. 7c). The dome also shows distinct salinity characteristics (Fig. 7d). The subsurface high-salinity core that exists along with the SMC (see “The high-salinity core” section) does not penetrate into the SLD. The near-surface salinity within the SLD is higher compared to the north but lower than that in the east, confirming its isolation from the influence of the SMC.

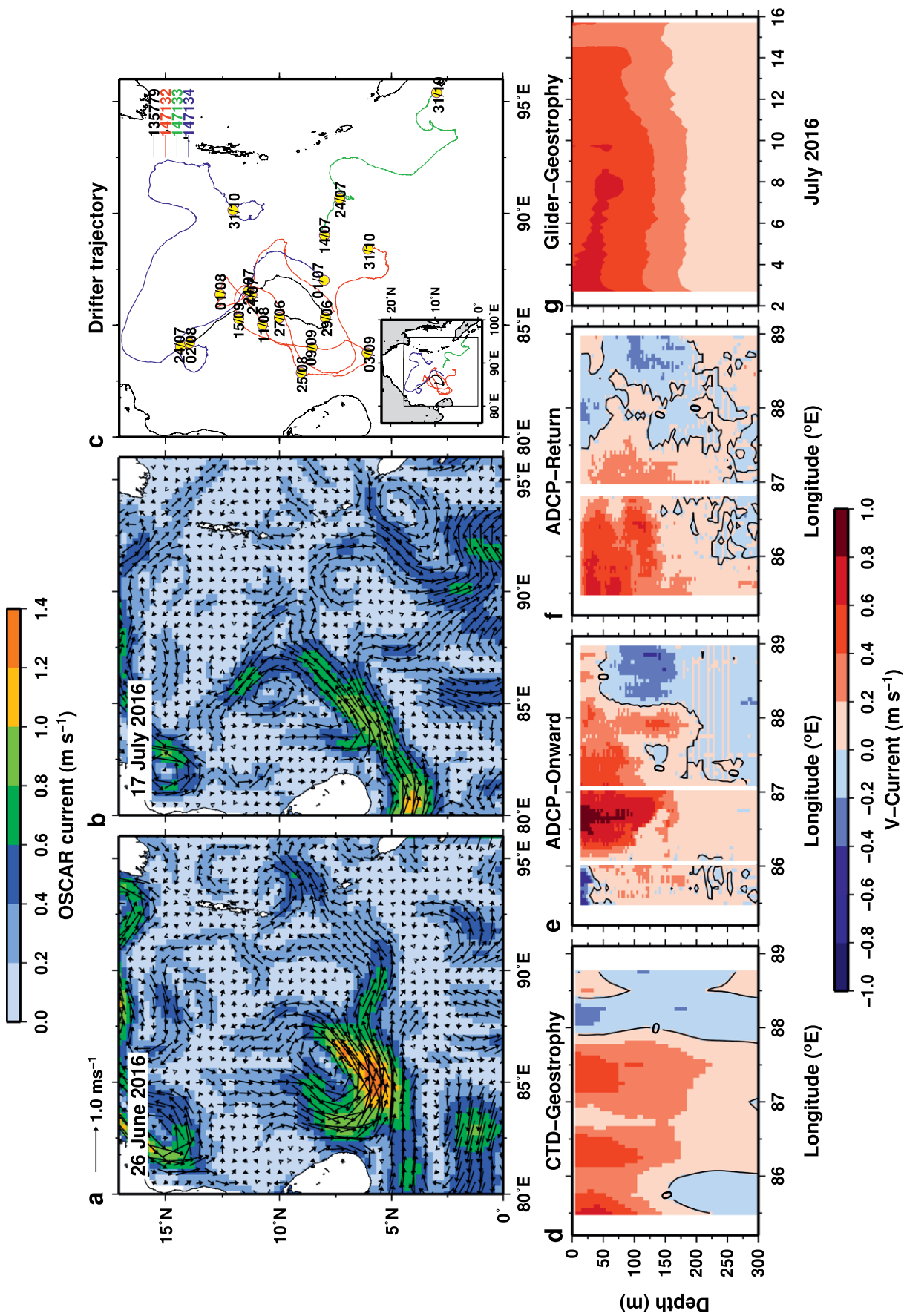
Along 8°N (Fig. 8), the thermocline (D20) within the dome is elevated relative to the region to the east. The CTD and glider sections in early July (Figs. 8a,b) correspond well during the season. The SLD moves

westward as the season progresses (Fig. 8c). It has been possible to delineate the changes in the east–west slope of the thermocline from early to mid-July because of these datasets generated by multiple instruments (Fig. 8d).

**The summer monsoon current.** The SMC flows eastward to the south of India (Schott et al. 1994) and then turns to flow into the BoB (Murty et al. 1992; Vinayachandran et al. 1999, 2013). The SMC was fully developed during the observation period with near-surface speeds of 0.5–1 m s<sup>−1</sup> (Figs. 9a,b). The circulation was characterized by a large cyclonic gyre to the east of Sri Lanka that was fully developed by the last week of June (Fig. 9a). The main axis of the SMC that flows northeastward into the BoB weakened and moved westward by mid-July; in the process, the gyre

► **FIG. 9.** The SMC. Surface currents from OSCAR (vector, m s<sup>−1</sup>) overlaid on current speed (shading) on (a) 26 Jun and (b) 17 Jul 2016. (c) Trajectories of four drifting buoys deployed during the cruise. (d) Meridional geostrophic current referenced to 500 dbar, calculated using ship CTD salinity measured at every 25° longitude along 8°N during 15–20 Jul 2016. (e) Meridional current measured using the ADCP during 30 Jun–4 Jul, and (f) 15–20 Jul 2016. (g) Time–depth meridional geostrophic current referenced to 500 dbar, at a nominal longitude of 87.5°E, calculated using SG534 and SG532 glider data (Table 1).





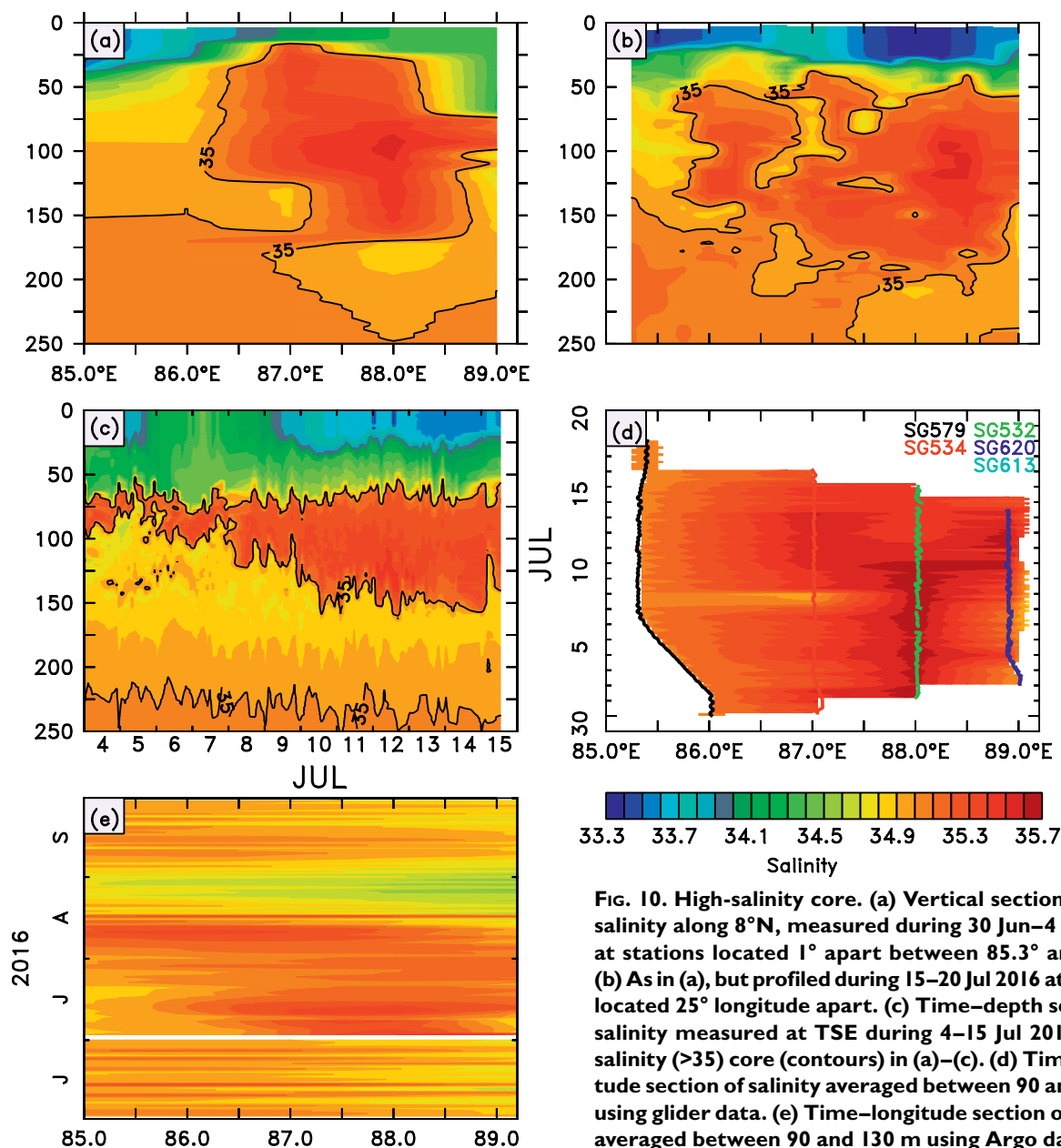


**FIG. 10. High-salinity core.** (a) Vertical section of CTD salinity along 8°N, measured during 30 Jun–4 Jul 2016, at stations located 1° apart between 85.3° and 89°E. (b) As in (a), but profiled during 15–20 Jul 2016 at stations located 25° longitude apart. (c) Time–depth section of salinity measured at TSE during 4–15 Jul 2016. High-salinity (>35) core (contours) in (a)–(c). (d) Time–longi-tude section of salinity averaged between 90 and 130 m using glider data. (e) Time–longitude section of salinity averaged between 90 and 130 m using Argo data.

elongated and shrank. Multiple filaments emanated from the SMC in different directions (Fig. 9b). One of them flowed toward the equator, another toward the east, one toward the northeast, and another continued to the southeast. One of the drifting buoys deployed during the cruise at TSW (8°N, 85.3°E) Fig. 3) on 29 June traversed along the cyclonic gyre (Fig. 9c) but two drifters continued toward India. The drifter deployed in the east (147132; Fig. 9c) moved southeast.

The BoBBLE section cut across the main branch of the SMC, and the TSE location was located on the outer edge of the filament flowing to the northeast. Geostrophic currents (Fig. 9d) showed high speeds ( $>0.5 \text{ m s}^{-1}$ ) near the surface and the northward flow

was restricted to depths shallower than 200 m, in agreement with previous observations (Wijesekera et al. 2016a). ADCP profiles confirm the shallow nature of the SMC (Figs. 9e,f). Between the two visits, the SMC weakened and shifted westward, the latter being consistent with the well-known process of Rossby wave propagation across the BoB (McCreary et al. 1996; Shankar et al. 2002). There is remarkable agreement between the ADCP data and geostrophic currents. The time–depth section of the geostrophic component of the SMC derived from glider data (Figs. 9e,g) shows decreasing velocities, consistent with the weakening and westward propagation of the SMC.

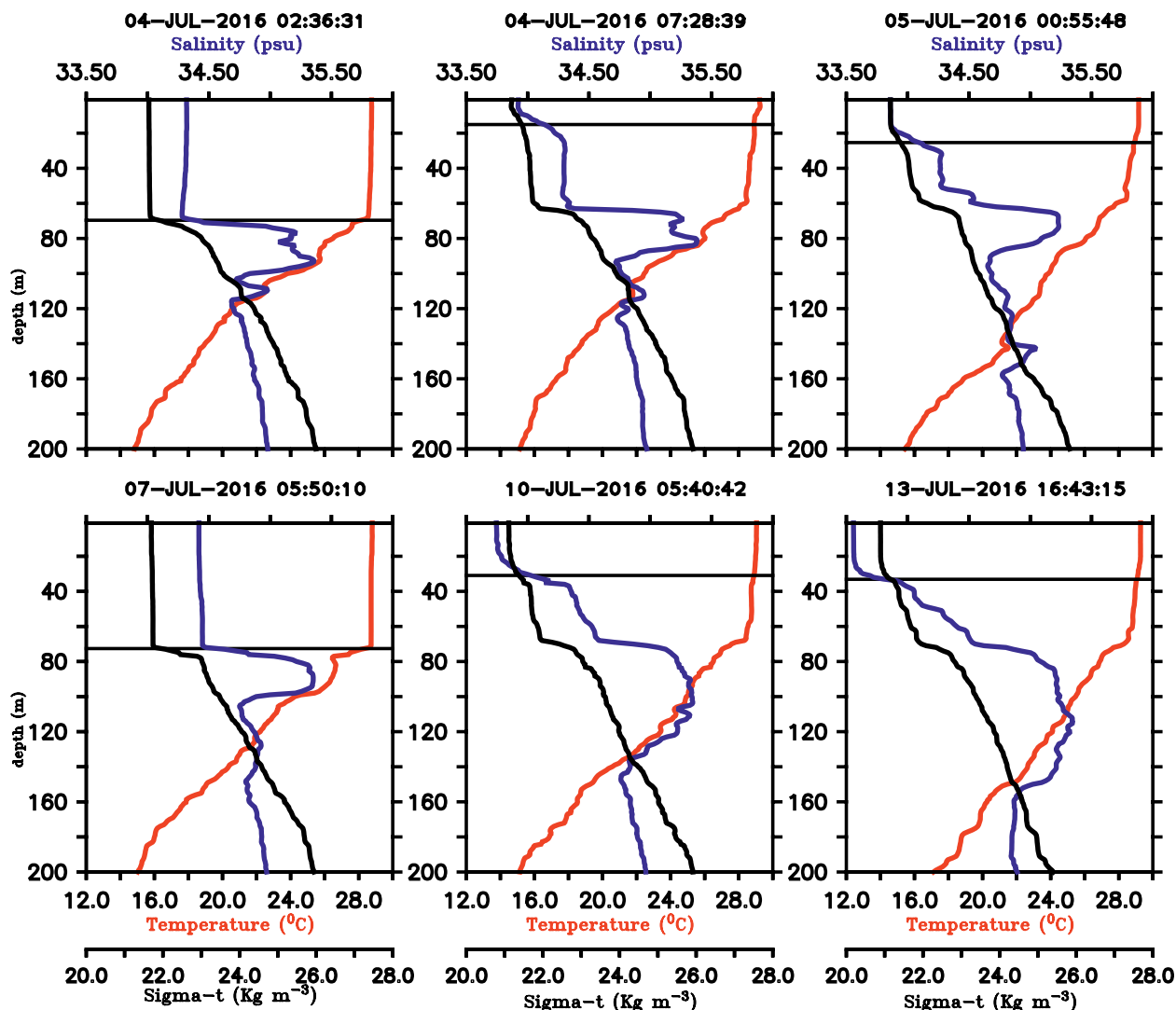


FIG. 11. Changes in the temperature and salinity characteristics of the upper layer due to freshening. (top) First freshening event (4–6 Jul 2016) described in the text. (bottom) Second freshening event (7–13 Jul 2016). Curves in all panels indicate temperature (red), salinity (blue), density (black), and MLD (horizontal lines). The date and time (UTC) of each profile is given above the respective panel. The situation (left) before and (middle) during the freshening event, and (right) the peak of the freshening event.

*The high-salinity core.* The SMC carries high-salinity water (>35.2 psu) from the Arabian Sea into the BoB. On encountering the lighter water of lower salinity, the Arabian Sea Water subducts beneath the latter. The intrusion of high-salinity (35–35.6 psu) water occurs below the mixed layer, to a maximum depth of about 200 m (Fig. 10). During 30 June–4 July (Fig. 10a), the high-salinity core was confined to 86°–89°E, between 25 and 175 m depth. At the eastern end (at 89°E), the core thinned to about 25 m thick. In contrast, at the western end, the profiles measured inside the SLD did not show the presence of Arabian Sea Water (Fig. 7d). At TSE, (Fig. 10b) the core thickened from about 25 m on 4 July to about

100 m on 15 July, suggesting a steady supply of high-salinity water during the observation period. Glider (Fig. 10d) and Argo (Fig. 10e) observations reveal temporal variations of the high-salinity core along the 8°N section.

*Freshening events and barrier-layer formation.* The 10-day time series at TSE captured two freshening events, one during 4–6 July and the other during 8–9 July (Fig. 10c). These events led barrier layers to form between the base of the upper isohaline layer and the base of the isothermal layer. The barrier layer formed rapidly during the first event. The SSS on 4 July dropped by 0.3 in 2 h, decreasing from 34.3 psu

at 0530 UTC to 33.9 psu by 0730 UTC (Fig. 11). Since there was no rain locally, this drop in salinity is attributed to horizontal advection. The mixed layer depth (MLD) decreased from 70 to 18 m, leading to the formation of a barrier layer that was about 50 m thick and had a temperature of 29°C. The upper layer warmed by about 0.3°C relative to the barrier layer below, during the following diurnal cycle.

The second event occurred more gradually; the SSS (MLD) decreased from 34.40 psu (75 m) on 7 July to 33.57 psu (35 m) on 13 July (Fig. 11). Consequently, a new barrier layer formed that was about 40 m thick. Periods of low SST coincided with higher salinity and the SST increased after both freshening events. There was also a distinct increase in the diurnal warming of SST after the freshening.

The barrier-layer formation at TSE is comparable to that in the northern bay, where the influence of river runoff and rainfall is more intense. Subsequent to the arrival of a fresh plume, the MLD decreased from 30 to 10 m during the 1999 summer monsoon (Vinayachandran et al. 2002), as a result of the decrease in SSS by about 4 psu over a period of 7 days. Observations during 2009 (Rao et al. 2011) also showed a similar decrease of SSS and MLD in one day. It is quite remarkable that even in the southern bay, where the direct influence of freshwater is much weaker compared to that in the north, the mixed layer

shallowing and barrier-layer formation occur to a comparable degree, suggesting that the behavior of the southern BoB mixed layer is comparable to that of the north during the summer monsoon.

**Submesoscale observations.** A uCTD was used for measuring vertical profiles of temperature and salinity while the ship was in transit (details are in the “BoBBLE field program” section). A uCTD section measured just after a spell of rain near TSE on 15 July 2016 (Fig. 12a) captured the spatial scale of a low-salinity pool that formed as result of the rain event. The salinity within the fresh pool was lower by 0.1 psu compared to the region outside, and the impact of rain was seen to a depth of 12 m. The width of this pool was 7 km. There was no apparent change in the temperature (Fig. 12b), and the isothermal layer extended all the way to about 40 m despite the isohaline layer being confined to the upper 10 m.

**Microstructure measurements.** Previous indirect dissipation measurements inferred from Argo floats in the central BoB suggested very low dissipation rates in the 250–500-m-depth range (Whalen et al. 2012). Recent direct dissipation measurements in the northern and central BoB (Jinadasa et al. 2016) show that the pycnocline is mostly decoupled from the low-salinity surface layer, with low turbulence in the

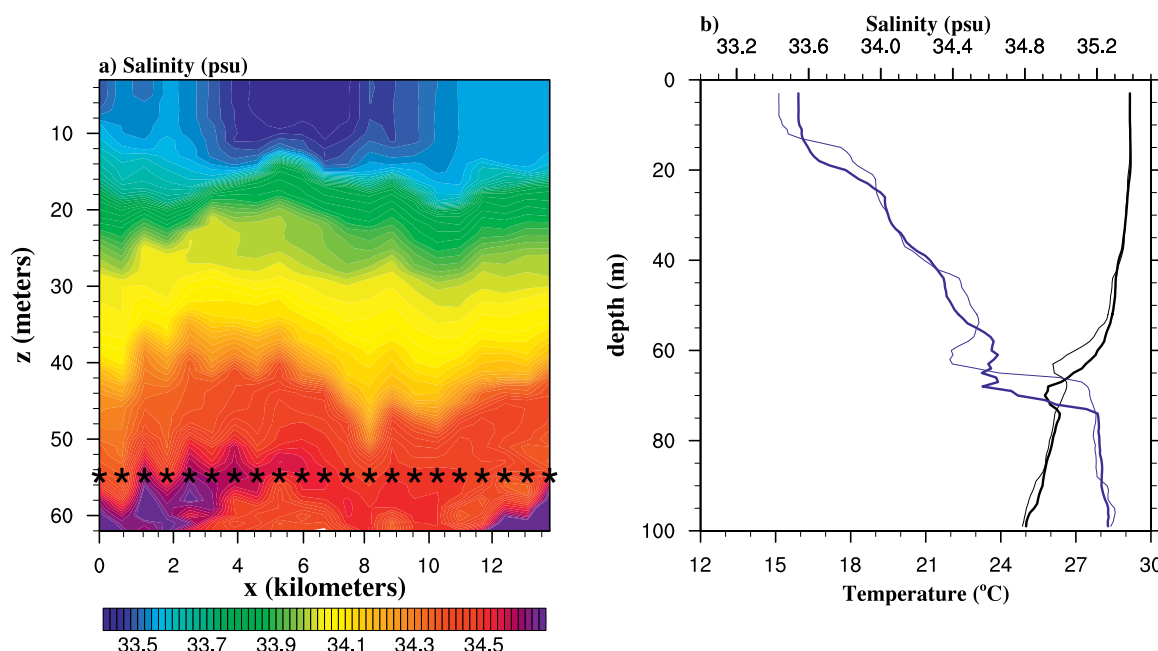


**FIG. 12.** uCTD observations of a rain-formed low-salinity pool. (a) Salinity along a 14-km section over which 21 vertical profiles were measured just after a spell of rain. Locations of uCTD profiles are indicated using asterisks marked at a depth of 55 m. Along the depth axis, the raw data are averaged into 1-m bins before plotting. (b) Vertical profiles of temperature (black) and salinity (blue) measured outside (at  $x = 2$  km, thick lines) and inside (at  $x = 6$  km, thin lines) the low-salinity pool.

deeper layer. Profiles from simultaneous casts of the VMP-250 (Figs. 13a–c) and the microstructure glider (Figs. 13d–f) at locations separated by a few kilometers suggest a shallow mixed layer (approximately 20 m thick) and a freshened upper layer (33.5 psu) compared to the thermocline region, where the salinity is 35.25 psu, confirming that the two platforms are sampling similar water columns. The 3-m binned profiles of turbulent kinetic energy dissipation rate  $\epsilon$  and vertical diffusivity  $K_z$  from the VMP (Fig. 13c) and the microstructure glider (Fig. 13f) suggest a sporadic and intermittent nature of the mixing in the water column. Within the mixed layer, the  $\epsilon$

and  $K_z$  were greater than  $10^{-8} \text{ W kg}^{-1}$  and  $10^{-4} \text{ m}^2 \text{ s}^{-1}$ , respectively. Below the mixed layer,  $\epsilon$  decreased to  $10^{-10} \text{ W kg}^{-1}$  and  $K_z$  reduced to  $10^{-6} \text{ m}^2 \text{ s}^{-1}$ . The microstructure data are consistent with the observations of Jinadasa et al. (2016) and Whalen et al. (2012).

**Biogeochemical observations.** LIGHT PENETRATION AND CHLOROPHYLL. The glider SG579 (Table 1) equipped with a PAR sensor provides a proxy for the shortwave radiation flux. A sample profile (Fig. 14) shows a rapid decrease in radiation flux in the top 1–2 m, associated with the absorption of the red light part of the spectrum. Below this level PAR decreases much more

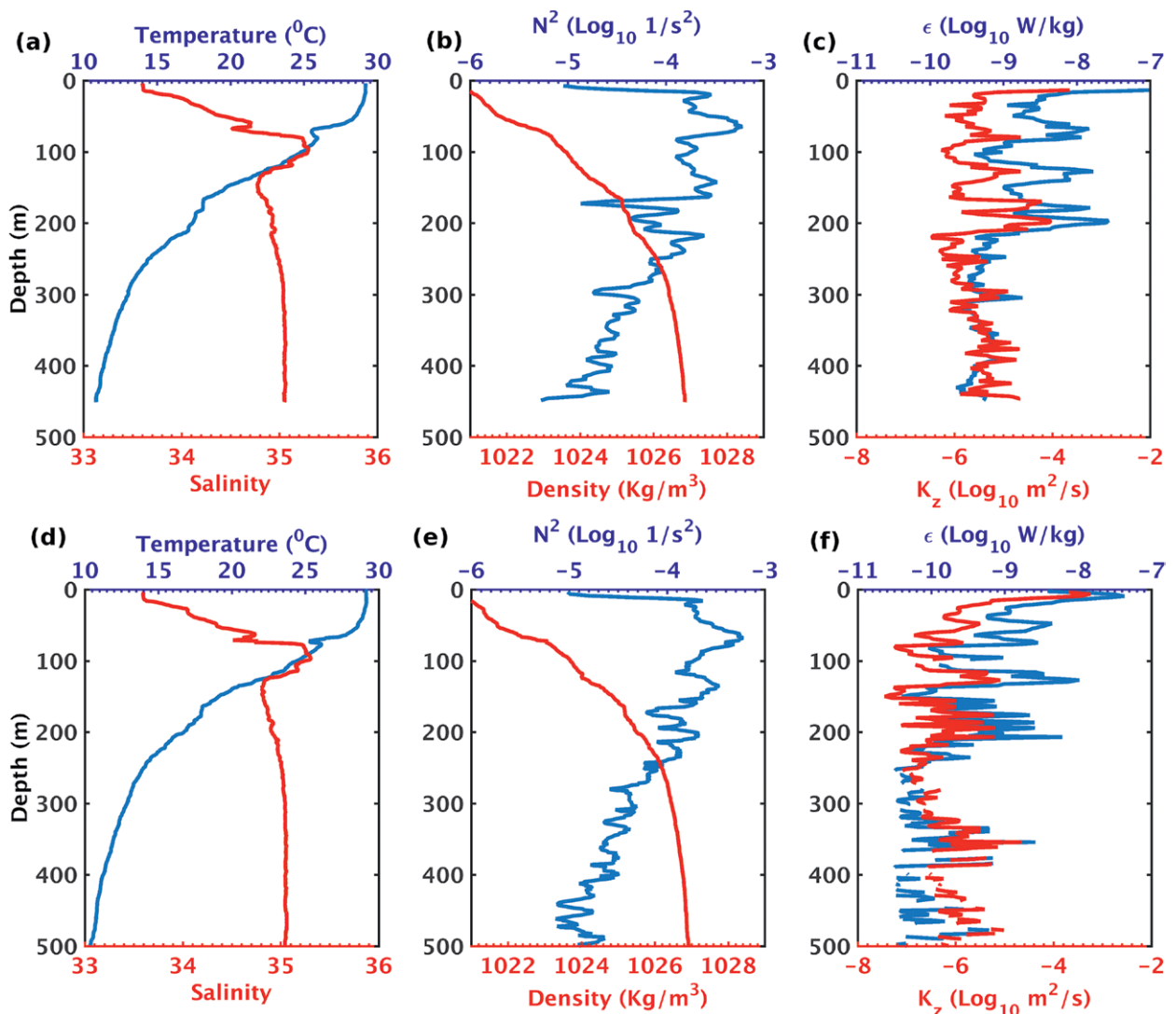


**FIG. 13.** Data from VMP-250 at 7°54'N and 89°06'E on 15 Jul 2016: (a) temperature (blue) and salinity (red), (b) squared Brunt–Väisälä frequency (blue) and density (red), and (c)  $\log_{10}$  of  $\epsilon$  (blue) and  $\log_{10}$  of  $K_z$  (red). Near-simultaneous data from glider SG613: (d) temperature (blue) and salinity (red), (e)  $N^2$  (blue) and density (red), and (f)  $\log_{10}$  of  $\epsilon$  (blue) and  $\log_{10}$  of  $K_z$  (red). The noise threshold of  $\epsilon = 10^{-10.5} \text{ W kg}^{-1}$ . The measured microstructure shear was used to infer  $\epsilon$  and  $K_z$  in the water column by assuming isotropic turbulence (Moum et al. 1995) and a mixing efficiency of 0.2 (Osborn 1980). The upper 10 m of the VMP-250 data has been removed to avoid contamination by the ship's wake.



slowly, associated with the absorption of the blue light part of the spectrum. A double exponential curve was fitted, producing a scale depth of 0.3 m for red light, and 18 m for blue light. Collocated measurements of chlorophyll concentration (Table 1) show a layer of chlorophyll below 30 m (green line in Fig. 14), with near-zero values above this. The effects of chlorophyll absorption of solar radiation, and any subsequent effect on SST, and through ocean–atmosphere interactions, a feedback onto precipitation, will be examined during the project.

**O<sub>2</sub> AND pCO<sub>2</sub>.** The dissolved oxygen at the surface ranged between 199 and 212  $\mu\text{mol kg}^{-1}$  with the eastern part of the transect showing relatively higher values (Fig. 15a). The surface pH (Fig. 15b), total alkalinity (Fig. 15c), and partial pressure of CO<sub>2</sub> (pCO<sub>2</sub>; Fig. 15e) exhibited a similar distribution. The pH had a range of 8.071–8.168 units, whereas total alkalinity varied between 2,172 and 2,295  $\mu\text{mol kg}^{-1}$ . Atmospheric CO<sub>2</sub> (pCO<sub>2</sub><sup>air</sup>) ranged between 386 and 409  $\mu\text{atm}$  (Fig. 15d), where higher concentrations were associated with the station at 10°N, 85.3°E (Fig. 3). This station also exhibited high pCO<sub>2</sub> (pCO<sub>2</sub><sup>w</sup>) with a range of 467–554  $\mu\text{atm}$ . The low surface pH in tandem with low alkalinity and high pCO<sub>2</sub> at this station suggest upwelled waters, presumably associated with the SMC. Overall, all sampling stations exhibited

high pCO<sub>2</sub> compared to the atmospheric mixing ratios, suggesting that the southern BoB is a possible source of CO<sub>2</sub> to the atmosphere during summer.

**SUMMARY AND OUTLOOK.** During a typical summer monsoon season, discrete cloud bands periodically form over the Indian Ocean and then migrate over the Asian landmass, culminating in rainfall there. Such cloud bands can be embedded in large-scale intraseasonal oscillations or manifest as synoptic monsoon depressions. The BoB is a key region for the formation and propagation of these atmospheric systems. Thus, the variability of rainfall over the Asian landmass during the monsoon is closely linked to the exchange of heat and moisture taking place over the Indian Ocean. Hence, understanding the detailed physical processes of ocean–atmosphere interaction over the Indian Ocean, and the BoB in particular, is crucial for understanding and the successful modeling and prediction of monsoon variability.

BoBBLE was motivated by this need and was designed to investigate oceanographic conditions and air–sea interaction over the hitherto little-known southern BoB during the summer monsoon. This paper outlines the preliminary results from the BoBBLE field program, which was aimed at collecting high-quality in situ observations from multiple platforms, including an ocean research ship, five ocean gliders, and seven specially configured Argo floats.

The BoBBLE observations were made during July 2016, during a suppressed phase of the BSISO when the ocean and atmosphere were being preconditioned for an impending active stage of the monsoon. During this period, which was characterized by intense solar radiation, the ocean warmed and exhibited strong diurnal variability. At the end of the BoBBLE observation period, atmospheric convection broke out over the southern BoB as part of the next, active phase of a northward-propagating BSISO. This active phase subsequently led to rainfall over India and the Asian landmass.

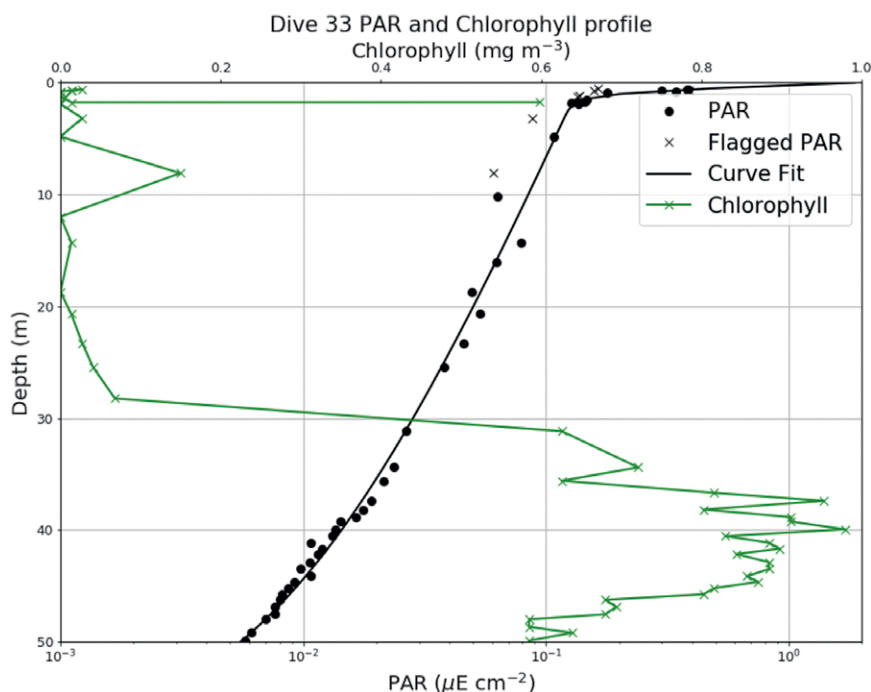


**FIG. 14.** PAR profile (black dots) from a sample dive from glider SG579, near midday on 6 Jul 2016. The best-fit double exponential curve is shown by the black line. Chlorophyll concentration is shown by the green crosses and line.

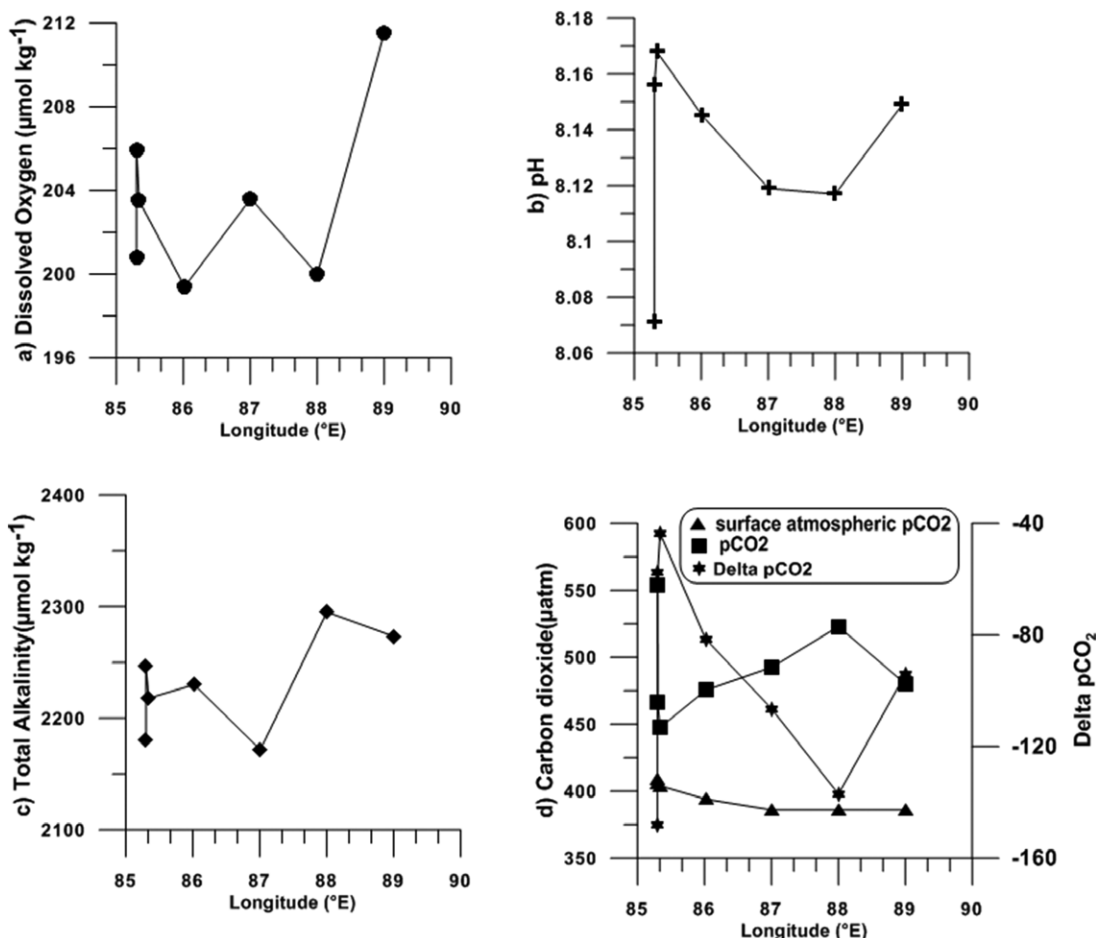


**FIG. 15. Spatial variation of surface biogeochemical properties during BoBBLE: (a) dissolved oxygen; (b) pH; (c) total alkalinity; and (d)  $p\text{CO}_2^{\text{air}}$ ,  $p\text{CO}_2^{\text{sw}}$ , and the difference in air–sea  $p\text{CO}_2$  concentration. Water sampling was carried out using an SBE CTD–rosette system fitted with 10-L Niskin bottles. Samples were collected along the 8°N transect at locations (red stars) denoted in Fig. 3**

The BoBBLE campaign has also made detailed observations of the major oceanographic features of the southern BoB. Using multiple in situ platforms, the spatial and temporal evolution of features such as the SLD and the high-salinity core in the SMC have been delineated using in situ datasets. Other observations include the formation of barrier layers in the southern BoB and details of the associated changes in the mixed layer. The physical processes involved in barrier-layer formation in the southern BoB contrast with those at work in the north.

The next challenge for the BoBBLE program is to incorporate the observational knowledge gained by the field program into physical process models and to determine the sensitivity of the monsoon system to ocean–atmosphere interactions in the southern BoB.

**ACKNOWLEDGMENTS.** BoBBLE is a joint MoES, India–NERC, U.K. program. The BoBBLE field program on board the R/V *Sindhu Sadhana* was funded by the Ministry

of Earth Sciences, government of India, under its Monsoon Mission program administered by the Indian Institute of Tropical Meteorology, Pune. We are indebted to the CSIR National Institute of Oceanography, Goa, India, for providing the R/V *Sindhu Sadhana* for BoBBLE. We greatly appreciate the encouragement by Dr. M. Rajeevan, secretary of MoES, and Dr. S. S. C. Shenoi, director of INCOIS, and the support and cooperation of Dr. P. S. Rao (NIO) and the captain, officers, and crew of the R/V *Sindhu Sadhana*. We thank Dr. D. Shankar (NIO), Dr. R. Venkatesan (NIOT), Dr. Tata Sudhakar (NIOT), Dr. Anil Kumar (NCOAR), Dr. M. Ravichandran (INCOIS), and their team, for their support for the field program. ASCAT wind data were obtained from IFREMER ([www.ifremer.fr/cersat/en/data/data.htm](http://www.ifremer.fr/cersat/en/data/data.htm)); NCEP data from NOAA ([www.esrl.noaa.gov/psd/](http://www.esrl.noaa.gov/psd/); Kalnay et al 1996); CERES downward longwave and shortwave radiation data from NASA (<http://ceres.larc.nasa.gov>); OSCAR data from NASA (<http://podaac.jpl.nasa.gov/CitingPODAAC>); AMSR-E products from Remote Sensing Systems ([www.remss.com/missions/amr](http://www.remss.com/missions/amr)); KALPANA OLR

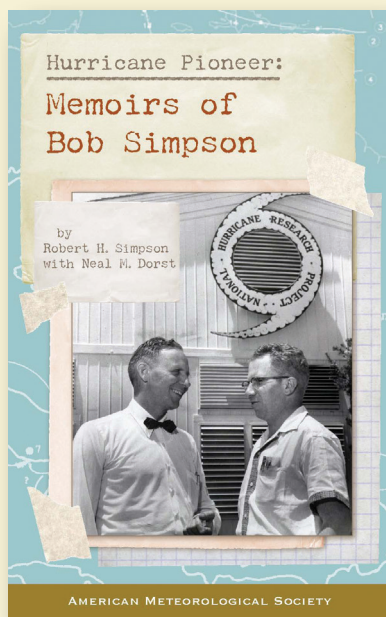
from the Indian Institute of Tropical Meteorology ([www.tropmet.res.in](http://www.tropmet.res.in)); TRMM rainfall data from NASA (<http://daac.gsfc.nasa.gov/precipitation>); MSLA from Copernicus Marine and Environment Monitoring Service (CMEMS; <http://marine.copernicus.eu/>); gridded Argo data from the Global Data Assembly Centre (Argo GDAC); and SEANOE and ERA winds, fluxes, and meteorological parameters from ECMWF ([www.ecmwf.int/en/research/climate-reanalysis/era-interim](http://www.ecmwf.int/en/research/climate-reanalysis/era-interim)). The core Argo profiles were collected and made freely available by the international Argo program and the national programs that contribute to it ([www.argo.ucsd.edu](http://www.argo.ucsd.edu), <http://argo.jcommops.org>). NPK was supported by NERC (NE/L010976/1). ASF, BGMW, and SCP were supported by the NERC BoBBLE project (NE/L013835/1, NE/L013827/1, NE/L013800/1). PNV was supported by the Ministry of Earth Sciences (MM/NERC-MoES-02/2014/002). Participation of all Indian scientists were supported by the MoES-BoBBLE project, and all others were supported by the NERC-BoBBLE Project. We thank three anonymous reviewers for their thoughtful and constructive comments on the manuscript.

## REFERENCES

- Bhat, G. S., and R. Narasimha, 2007: Indian summer monsoon experiments. *Curr. Sci.*, **93**, 153–164.
- , and Coauthors, 2001: BOBMEX: The Bay of Bengal Monsoon Experiment. *Bull. Amer. Meteor. Soc.*, **82**, 2217–2243, [https://doi.org/10.1175/1520-0477\(2001\)082<2217:BTBOBM>2.3.CO;2](https://doi.org/10.1175/1520-0477(2001)082<2217:BTBOBM>2.3.CO;2).
- Boyer, T. P., and Coauthors, 2013: World Ocean Database 2013. NOAA Atlas NESDIS 72, 209 pp.
- Das, U., P. N. Vinayachandran, and A. Behara, 2016: Formation of the southern Bay of Bengal cold pool. *Climate Dyn.*, **47**, 2009–2023, <https://doi.org/10.1007/s00382-015-2947-9>.
- Dupuis, H., C. Guerin, D. Hauser, A. Weill, P. Nacass, W. M. Drennan, S. Cloché, and H. C. Graber, 2003: Impact of flow distortion corrections on turbulent fluxes estimated by the inertial dissipation method during the FETCH experiment on R/V *L'Atalante*. *J. Geophys. Res.*, **108**, 8064, <https://doi.org/10.1029/2001JC001075>.
- Edson, J. B., A. A. Hinton, K. E. Prada, J. E. Hare, and C. W. Fairall, 1998: Direct covariance flux estimates from mobile platforms at sea. *J. Atmos. Oceanic Technol.*, **15**, 547–562, [https://doi.org/10.1175/1520-0426\(1998\)015<0547:DCFEFM>2.0.CO;2](https://doi.org/10.1175/1520-0426(1998)015<0547:DCFEFM>2.0.CO;2).
- Fairall, C., A. White, J. Edson, and J. Hare, 1997: Integrated shipboard measurements of the marine boundary layer. *J. Atmos. Oceanic Technol.*, **14**, 338–359, [https://doi.org/10.1175/1520-0426\(1997\)014<0338:ISMOTM>2.0.CO;2](https://doi.org/10.1175/1520-0426(1997)014<0338:ISMOTM>2.0.CO;2).
- Gadgil, S., 2003: The Indian monsoon and its variability. *Annu. Rev. Earth Planet. Sci.*, **31**, 429–467, <https://doi.org/10.1146/annurev.earth.31.100901.141251>.
- Jain, V., and Coauthors, 2017: Evidence for the existence of Persian Gulf Water and Red Sea Water in the Bay of Bengal. *Climate Dyn.*, **48**, 3207–3226, <https://doi.org/10.1007/s00382-016-3259-4>.
- Jinadasa, S. U. P., I. Lozovsky, J. Planella-Morató, J. D. Nash, J. A. MacKinnon, A. J. Lucas, H. W. Wijesekera, and H. J. S. Fernando, 2016: Ocean turbulence and mixing around Sri Lanka and in adjacent waters of the northern Bay of Bengal. *Oceanography*, **29** (2), 170–179, <https://doi.org/10.5670/oceanog.2016.49>.
- Joseph, P. V., K. P. Sooraj, C. A. Babu, and T. P. Sabin, 2005: A cold pool in the Bay of Bengal and its interaction with the active-break cycle of monsoon. *CLIVAR Exchanges*, No. 34, International CLIVAR Project Office, Southampton, United Kingdom, 10–12.
- Kalnay, E., and Coauthors, 1996: The NCEP/NCAR 40-Year Reanalysis Project. *Bull. Amer. Meteor. Soc.*, **77**, 437–471, [https://doi.org/10.1175/1520-0477\(1996\)077<0437:TNYRP>2.0.CO;2](https://doi.org/10.1175/1520-0477(1996)077<0437:TNYRP>2.0.CO;2).
- Lee, C. M., and Coauthors, 2016: Collaborative observations of boundary currents, water mass variability, and monsoon response in the southern Bay of Bengal. *Oceanography*, **29** (2), 102–111, <https://doi.org/10.5670/oceanog.2016.43>.
- Lee, J.-Y., B. Wang, M. C. Wheeler, X. Fu, D. E. Waliser, and I.-S. Kang, 2013: Real-time multivariate indices for the boreal summer intraseasonal oscillation over the Asian summer monsoon region. *Climate Dyn.*, **40**, 493–509, <https://doi.org/10.1007/s00382-012-1544-4>.
- Matthews, A. J., D. B. Baranowski, K. J. Heywood, P. J. Flatau, and S. Schmidt, 2014: The surface diurnal warm layer in the Indian Ocean during CINDY/DYNAMO. *J. Climate*, **27**, 9101–9122, <https://doi.org/10.1175/JCLI-D-14-00222.1>.
- , and Coauthors, 2015: BoBBLE: Bay of Bengal boundary layer experiment. *CLIVAR Exchanges*, No. 68, International CLIVAR Project Office, Southampton, United Kingdom, 38–42.
- McCreary, J. P., W. Han, D. Shankar, and S. R. Shetye, 1996: Dynamics of the East India Coastal Current: 2. Numerical solutions. *J. Geophys. Res.*, **101**, 13 993–14 010, <https://doi.org/10.1029/96JC00560>.
- McPhaden, M. J., and Coauthors, 2009: RAMA: The Research Moored Array for African–Asian–Australian Monsoon Analysis and Prediction. *Bull. Amer. Meteor. Soc.*, **90**, 459–480, <https://doi.org/10.1175/2008BAMS2608.1>.
- Moum, J. N., M. C. Gregg, R. C. Lien, and M. E. Carr, 1995: Comparison of turbulence kinetic energy dissipation



- rate estimates from two ocean microstructure profilers. *J. Atmos. Oceanic Technol.*, **12**, 346–366, [https://doi.org/10.1175/1520-0426\(1995\)012<0346:COTKED>2.0.CO;2](https://doi.org/10.1175/1520-0426(1995)012<0346:COTKED>2.0.CO;2).
- Murty, V. S. N., Y. V. B. Sarma, D. P. Rao, and C. S. Murty, 1992: Water characteristics, mixing and circulation in the Bay of Bengal during southwest monsoon. *J. Mar. Res.*, **50**, 207–228, <https://doi.org/10.1357/002224092784797700>.
- Nair, A. K. M., K. Rajeev, S. Sijikumar, and S. Meenu, 2011: Characteristics of a persistent pool of inhibited cloudiness and its genesis over the Bay of Bengal associated with the Asian summer monsoon. *Ann. Geophys.*, **29**, 1247–1252, <https://doi.org/10.5194/angeo-29-1247-2011>.
- Osborn, T. R., 1980: Estimates of the local rate of vertical diffusion from dissipation measurements. *J. Phys. Oceanogr.*, **10**, 83–89, [https://doi.org/10.1175/1520-0485\(1980\)010<0083:EOTLRO>2.0.CO;2](https://doi.org/10.1175/1520-0485(1980)010<0083:EOTLRO>2.0.CO;2).
- Rao, S. A., and Coauthors, 2011: Modulation of SST, SSS over northern Bay of Bengal on ISO time scale. *J. Geophys. Res.*, **116**, C09026, <https://doi.org/10.1029/2010JC006804>.
- Saji, N. H., B. N. Goswami, P. N. Vinayachandran, and T. Yamagata, 1999: A dipole mode in the tropical Indian Ocean. *Nature*, **401**, 360–363, <https://doi.org/10.1038/43854>.
- Schott, F., J. Reppin, J. Fischer, and D. Quadfasel, 1994: Currents and transports of the Monsoon Current south of Sri Lanka. *J. Geophys. Res.*, **99**, 25 127–25 141, <https://doi.org/10.1029/94JC02216>.
- Shankar, D., P. N. Vinayachandran, and A. S. Unnikrishnan, 2002: The monsoon current in the north Indian Ocean. *Prog. Oceanogr.*, **52**, 63–120, [https://doi.org/10.1016/S0079-6611\(02\)00024-1](https://doi.org/10.1016/S0079-6611(02)00024-1).
- , S. R. Shetye, and P. V. Joseph, 2007: Link between convection and meridional gradient of sea surface temperature in the Bay of Bengal. *J. Earth Syst. Sci.*, **116**, 385–406, <https://doi.org/10.1007/s12040-007-0038-y>.
- Shenoi, S. S. C., D. Shankar, and S. R. Shetye, 2002: Differences in heat budgets of the near-surface Arabian Sea and Bay of Bengal: Implications for the summer monsoon. *J. Geophys. Res.*, **107**, 5–1, <https://doi.org/10.1029/2000JC000679>.
- Vinayachandran, P. N., and T. Yamagata, 1998: Monsoon response of the sea around Sri Lanka: Generation of thermal domes and anticyclonic vortices. *J. Phys. Oceanogr.*, **28**, 1946–1960, [https://doi.org/10.1175/1520-0485\(1998\)028<1946:MRO TSA>2.0.CO;2](https://doi.org/10.1175/1520-0485(1998)028<1946:MRO TSA>2.0.CO;2).
- , Y. Masumoto, T. Mikawa, and T. Yamagata, 1999: Intrusion of the southwest monsoon current into the Bay of Bengal. *J. Geophys. Res.*, **104**, 11 077–11 085, <https://doi.org/10.1029/1999JC900035>.
- , V. S. N. Murty, and V. Ramesh Babu, 2002: Observations of barrier layer formation in the Bay of Bengal during summer monsoon. *J. Geophys. Res.*, **107**, 8018, <https://doi.org/10.1029/2001JC000831>.
- , D. Shankar, S. Vernekar, K. K. Sandeep, P. Amol, C. P. Neema, and A. Chatterjee, 2013: A summer monsoon pump to keep the Bay of Bengal salty. *Geophys. Res. Lett.*, **40**, 1777–1782, <https://doi.org/10.1002/grl.50274>.
- Webster, P. J., and Coauthors, 2002: The JASMINE pilot study. *Bull. Amer. Meteor. Soc.*, **83**, 1603–1630, <https://doi.org/10.1175/BAMS-83-11-1603>.
- Weller, R. A., E. F. Bradley, J. B. Edson, C. W. Fairall, I. M. Brooks, M. J. Yelland, and R. W. Pascal, 2008: Sensors for physical fluxes at the sea surface: Energy, heat, water, salt. *Ocean Sci.*, **4**, 247–263, <https://doi.org/10.5194/os-4-247-2008>.
- Whalen, C. B., L. D. Talley, and J. A. MacKinnon, 2012: Spatial and temporal variability of global ocean mixing inferred from Argo profiles. *Geophys. Res. Lett.*, **39**, L18612, <https://doi.org/10.1029/2012GL053196>.
- Wijesekera, H. W., W. J. Teague, D. W. Wang, E. Jarosz, T. G. Jensen, S. U. P. Jinadasa, H. J. S. Fernando, and Z. R. Hallock, 2016a: Low-frequency currents from deep moorings in the southern Bay of Bengal. *J. Phys. Oceanogr.*, **46**, 3209–3238, <https://doi.org/10.1175/JPO-D-16-0113.1>.
- , and Coauthors, 2016b: ASIRI: An ocean–atmosphere initiative for Bay of Bengal. *Bull. Amer. Meteor. Soc.*, **97**, 1859–1884, <https://doi.org/10.1175/BAMS-D-14-00197.1>.
- , and Coauthors, 2016c: Observations of currents over the deep southern Bay of Bengal—With a little luck. *Oceanography*, **29** (2), 112–123, <https://doi.org/10.5670/oceanog.2016.44>.
- Xie, S.-P., H. Xu, N. H. Saji, Y. Wang, and W. T. Liu, 2006: Role of narrow mountains in large-scale organization of Asian monsoon convection. *J. Climate*, **19**, 3420–3429, <https://doi.org/10.1175/JCLI3777.1>.
- Yu, L., 2003: Variability of the depth of the 20°C isotherm along 6°N in the Bay of Bengal: Its response to remote and local forcing and its relation to satellite SSH variability. *Deep-Sea Res. II*, **50**, 2285–2304, [https://doi.org/10.1016/S0967-0645\(03\)00057-2](https://doi.org/10.1016/S0967-0645(03)00057-2).



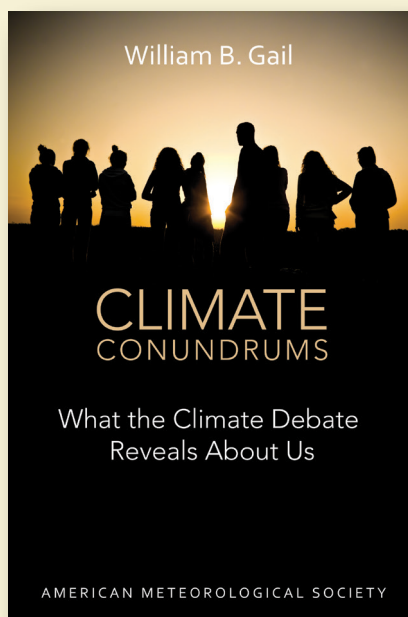
## HURRICANE PIONEER

### Memoirs of Bob Simpson

Robert H. Simpson with Neal M. Dorst

In 1951, Bob Simpson rode a plane directly into the wall of a hurricane—just one of his many pioneering explorations. This autobiography of the first director of the National Hurricane Research Project and co-creator of the Saffir-Simpson Hurricane Scale starts with childhood remembrance and ends in first-hand account of a revolutionary

© 2014, PAPERBACK  
ISBN: 978-1-935704-75-1  
LIST \$30 MEMBER \$20



## CLIMATE CONUNDRUMS

### What the Climate Debate Reveals About Us

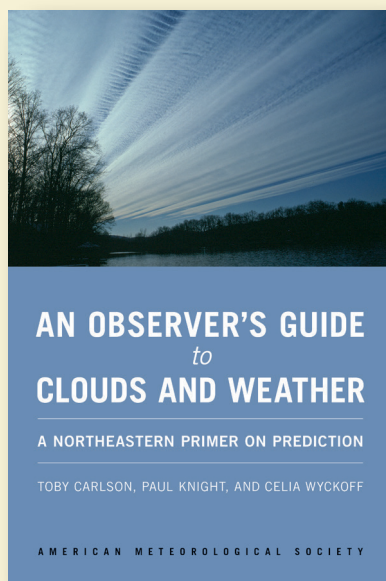
William B. Gail

This is a journey through how we think, individually and collectively, derived from the climate change debate. With wit and wisdom, Gail explores several questions: Can we make nature better? Could science and religion reconcile? Insights from such issues can help us better understand who we are and help

© 2014, PAPERBACK  
ISBN: 978-1-935704-74-4  
LIST \$30 MEMBER \$20

Browse online at  
[ametsoc.org/bookstore](http://ametsoc.org/bookstore)

**FREE SHIPPING**  
for AMS Members!



## AN OBSERVER'S GUIDE TO CLOUDS AND WEATHER

### A Northeast Primer on Prediction

Toby Carlson, Paul Knight, and Celia Wyckoff

With help from Penn State experts, start at the beginning and go deep. This primer for enthusiasts and new students alike will leave you with both refined observation skills and an understanding of the complex science behind the weather: the ingredients for making reliable predictions of your own.

© 2014, PAPERBACK  
ISBN: 978-1-935704-58-4  
LIST \$35 MEMBER \$20



**AMS BOOKS**

AMS Books are available to groups and booksellers, and desk copies may be obtained, through our distributor The University of Chicago Press: 1-800-621-2736 or [custserv@press.uchicago.edu](mailto:custserv@press.uchicago.edu).